

Intermodal entanglement in a quantum optical model of HHG due to the back-action on the driving field

Ákos Gombköt,¹ Peter Adam,^{1,2} David Theidel,³ and Tamás Kiss¹

¹*HUN-REN Wigner Research Centre for Physics,
Konkoly-Thege M. út 29-33, H-1121 Budapest, Hungary*

²*Institute of Physics, University of Pécs, Ifjúság útja 6, H-7624 Pécs, Hungary*

³*Laboratoire d'Optique Appliquée (LOA), CNRS, École polytechnique,
ENSTA, Institut Polytechnique de Paris, Palaiseau, France*

Preparation of nonclassical light with special quantum properties is essential for quantum technologies. High-harmonic generation (HHG) is a process which not only enables the creation of attosecond pulses but also has the potential to generate light with intricate quantum properties. In a recent experiment [1], nonclassical inter-harmonic correlations have been measured from a HHG source. In this work, we theoretically investigate entanglement between different harmonics within an effective quantum optical model. This model implements a significant degree of simplification regarding the processes within the target material, treating the material through susceptibilities, as it is usual in quantum optics. Such an approach yields a general description of HHG, permitting the implications that can be derived within it to hold broadly. We find that entanglement is produced as a result of the often neglected back-action. We can qualitatively reproduce experimentally measured nonclassicalities, which suggests that intermodal entanglement can, to an extent, be considered a universal phenomenon associated with HHG, rather than a result of using specific material targets.

I. INTRODUCTION

Established techniques for generating quantum light at optical frequencies [2, 3] typically rely on nonlinear optical processes [4]. These processes involve the nonlinear optical response of materials, often described using a perturbative approach, where the induced polarization is proportional to a low-order power of the applied electric field [5]. These models all share the common feature of incorporating the material response through parameters that characterize the effective interaction between the involved modes. The resulting Hamiltonian is typically used to describe quantum optical processes, such as second- or third-harmonic generation or parametric down-conversion.

The process of high-harmonic generation (HHG) includes a very intense electromagnetic pulse generating radiation across a wide spectrum of higher frequencies [6–9]. As such, HHG is a fundamental source of ultrashort pulses in attophysics. Due to the non-perturbative, strong-field effects inherent in HHG, the detailed description is highly complicated. Historically, a quantum optical description of HHG was given for the first time by J. Bergou and S. Varró in 1981 [10]. Since then, various approaches have been proposed in the literature for incorporating quantum features of the participating fields [11–17]. After 2020, there has been a significant surge of interest toward this topic, marking the transition of the quantum optical investigation of HHG from a niche topic into a promising research area. For reviews of research directions, techniques and methods, see Refs. [4, 18–30].

In recent years, both theoretical and experimental results suggest that the quantum optics of high-intensity light-matter interaction—specifically of HHG—have remarkable potential in developing a source of unusual nonclassical photonic states. Details of experimen-

tal setups and measured results may be found in e.g. Refs. [1, 16, 30–37]. Theoretical research typically uses models where the target material and either the driving field or the harmonic modes are quantized. This naturally leads to approximations, most often non-depletion for either the driving field, or for the initial material quantum state. The theoretical calculations suggest that large-scale, multimode correlated [38–50] and squeezed [10, 24, 38, 40, 46, 49, 51–55] states, as well as highly displaced, intensive cat-states [29, 41, 42, 48, 56–62], and other quantum states characterized by nonclassical photon-statistic [38, 39, 49, 50, 52, 63–65] may be generated as a result of HHG. The quantum properties of harmonics generated under coherent-state excitation have been theoretically studied in e.g. Refs. [38, 39, 52, 53, 66], while the modifications in the photon statistics of the driving field has been explored in Refs. [31, 67–69]. HHG involving non-coherent state driving pulses have also been extensively studied recently [32, 70–82], together with the impact that the initial quantum state of, and specifically initial correlations in the target material, has on the resulting photonic properties [46, 51, 54, 83–87]. Brief summaries of current research can be found in sources such as Refs. [88–94].

Theoretical prediction of nontrivial cross-correlations emerging between harmonics have been made in earlier works. For a monochromatically driven two-level system, harmonic-harmonic correlations have been analyzed in Refs. [38, 39]. Afterward, a calculation involving one-photon ionization and free-electron dynamics found a necessity for correlations between harmonics to arise [45]. Furthermore, an analysis of HHG from correlated many-atom systems point to strong positive correlation emerging between harmonic photons [44].

Questions regarding the presence of entanglement, of course, needs to be treated separately, and with care.

While entanglement has been found to emerge during HHG between electron states and light [49, 50], and between the excitation mode and harmonic modes [46–48], the focal point of our current work concerns the harmonic-harmonic entanglement. Using rather general physical considerations, and without relying on a particular Hamiltonian, it was shown in Ref. [42], that during the process of HHG, after a conditioning, all harmonic modes become naturally entangled. A more detailed mathematical discussion of these results, with emphasis on the conditioning, can be found in Ref. [43]. These methods have also been applied for calculations involving semiconductor targets [41]. According to these papers, the entanglement is such, that measuring one mode can leave the entanglement of the other modes intact, suggesting the ability of using HHG for generating high dimensional optical cluster-type multipartite entangled states, useful for measurement-based quantum computation [95, 96]. On one hand, this raises the possibility of applications, and on the other hand, a solid theoretical foundation of the results, together with a limit of validity, is highly desirable. A different direction of research [40] found that transitions between different laser-dressed states of the material system can ultimately generate similar entanglement between different harmonics. A key consideration there was the abandonment of the coherent-state-product ansatz, which we will also build upon.

In a recent experiment [1], nonclassical intermodal correlations have been reported between pairs of harmonic modes. The experimental measurement involved three different material systems: Si, ZnO, and GaAs. One interpretation of the emerging nonclassicalities is based on the presence of entanglement between Gaussian states [35]. Nevertheless, the experimental results naturally raises the question of whether the measured nonclassical correlations between harmonic modes indeed correspond to entanglement. Further, it would be of theoretical interest and of experimental relevance to understand whether the nonclassicalities are specific to these materials, to semiconductors in general, or are broadly material-independent, universal features of HHG?

In order to answer this question, we turn to a recently introduced effective model for HHG [97], which considers both the driving field and the harmonics as quantized objects, while making minimal assumptions about the material target. Such an approach allows for providing a qualitative answer to this question by presenting approximate, analytical results. We show that in a consistent treatment of the dynamics, incorporating the depletion of the excitation mode results in a natural deviation from the coherent-state product ansatz, and entanglement within the harmonics. We use our results to qualitatively interpret the experimental results in [1]. In some respect we reinforce the results in Ref. [42], that is, we show that entanglement appear as a result of the depletion in the driving field, without conditioning, and without using heuristic assumptions. While serving as a justification for the approach in [42], our results can also

be used to delineate its validity. In our effective model, the depletion in the driving field mode is incorporated exactly. Our approach is, in some sense, complementary to the research direction in which the quantum dynamics of materials is to be considered in an exact manner [40, 98].

Our paper is organized as follows: In section II, we introduce an effective quantum optical model, along with the assumptions implicit within it. In section III, we present the dynamical equations for the quantum state of the electromagnetic field. Analytical results obtained through a perturbative approach are given in section IV. The interpretation of these results, applied to both an idealized perturbative and nonperturbative setup, as well as a qualitative fitting of parameters to experimental data has been given in Sec. V. A summary of our work is presented in Sec. VI.

II. MODEL

In any model of HHG, there are three key elements: the excitation, the material target, and the harmonic radiation. For first-principle calculations, all three of these must be considered in a quantized framework, which, however, presents an extremely challenging problem. Therefore, here we consider the material to be a classical continuum, represented solely through effective susceptibilities. In contrast, both the driving pulse and the scattered harmonics are represented as quantized modes.

Following this approach, we consider a Hamiltonian introduced in [97] to describe the process of HHG

$$H = \hbar\omega A^\dagger A + \hbar\omega \sum_n n a_n^\dagger a_n + \hbar \sum_n \chi_n [A^n a_n^\dagger + (A^\dagger)^n a_n], \quad (1)$$

where $A^{(\dagger)}$ are the creation/annihilation operators associated with the pump mode of frequency ω , and $a_n^{(\dagger)}$ are the creation/annihilation operators of the harmonic mode indexed with n , of frequency $n\omega$. The n indices are a subset of positive integers, specifically $n \in \{2, \dots, N\} \subset \mathbb{N}^+$, and $\chi_n \in \mathbb{R}$ denotes the n th order susceptibility of the material. Practically N corresponds to the cutoff harmonic order.

This Hamiltonian describes a physical process in which n photons are absorbed from the driving field's mode and simultaneously a photon is emitted into the corresponding n th harmonic mode. The corresponding Hermitian conjugate term describes the inverse process. This interaction term is a plausible description of HHG if the electrons return to their initial state after the interaction, meaning that energy is effectively not stored in the matter, it being responsible only for mediating the interaction between modes. Consequently, effective energy transfer happens solely between the pump field and harmonic modes, corresponding to the conservation of the energy of the electromagnetic field. The assumption of

a single electromagnetic mode representing the excitation is commonly used in quantum optics. The Hamiltonian does not include harmonic-harmonic interactions, as the harmonic modes are typically lowly populated, hence nonlinear interactions between them are weak. Whenever this Hamiltonian is applied to describe a concrete realization of HHG processes, the fitting can be performed by adjusting the susceptibilities in this model. In a typical HHG process, some of the outgoing modes, e.g., the ones with even indices, are missing or negligible, which can be taken into account by choosing the corresponding susceptibilities to be zero. The model of Eq. (1) opens the possibility of gaining analytical insight into the emergence of non-classicality and intermodal correlations solely due to the back-action on the driving field.

The resulting zeroth-order approximate solution of the Schrödinger-equation, governed by this Hamiltonian, reads

$$|\Psi^{(0)}(t)\rangle = \underbrace{|\alpha_0 e^{-i\omega t}\rangle}_{\alpha(t)} \otimes \prod_{n=2}^N \underbrace{|-it\chi_n \alpha_0^n e^{-in\omega t}\rangle}_{{\beta}_n(t)}. \quad (2)$$

assuming initial condition of the system

$$|\Psi(0)\rangle = |\alpha_0\rangle \otimes |0\rangle_2 \otimes \cdots \otimes |0\rangle_N. \quad (3)$$

The $|\Psi^{(0)}(t)\rangle$ zero-order solution corresponds to the assumption of non-depleting coherent excitation with amplitude α_0 and emerging harmonics in coherent states with linearly increasing amplitudes. This solution has been the foundation of further considerations in, for example, Refs. [43, 56, 71, 75]. It is easy to see that since the quantum state can be written as a product of coherent states, the zero-order solution does not contain entanglement or intermodal cross-correlations. However, these have been measured [1], and theoretically predicted [38], hence, it is important to investigate higher orders.

III. DYNAMICAL EQUATIONS

In this section, we express the dynamical equations governing the time-evolution of quantum states in a way that is conducive to further analysis. Our objective is to capture the leading deviations from the uncorrelated coherent-state product, as expressed in Eq. (2), induced by the time-evolution under Hamiltonian (1). For this purpose, we prepare a perturbative calculation, by an appropriate unitary transformation and by introducing a suitable interaction picture.

Our aim is to use transformations that ultimately lead to the perturbative results naturally being expressed in the basis

$$|\alpha(t), J\rangle \otimes \prod_{n=2}^N |\beta_n(t), j_n\rangle_n \quad J, j_n \in \mathbb{N}. \quad (4)$$

Here, and later, $|x, k\rangle$ denotes the displaced number-state $\mathcal{D}(x)|k\rangle$. Note that with parameters $J = 0$, $\{j_n = 0\}_n$,

the state corresponds to Eq. (2). Keeping the above in mind, we apply a time-dependent unitary transformation to transform Eq. (2) to the vacuum-state product

$$|\Psi^{(0)}(t)\rangle = e^{\Lambda(t)} |\Psi^{(0)}(t)\rangle = |0\rangle \otimes \prod_{n=2}^N |0\rangle_n, \quad (5)$$

where the Λ operator reads

$$\Lambda(t) = - \left(\alpha_0 e^{-i\omega t} A^\dagger - \alpha_0^* e^{i\omega t} A \right) - \sum_{n=2}^N \left((-it\chi_n \alpha_0^n e^{-in\omega t}) a_n^\dagger - (it\chi_n \alpha_0^{*n} e^{in\omega t}) a_n \right). \quad (6)$$

Applying this transformation to the Schrödinger-equation governed by Hamiltonian of Eq. (1), we get the dynamical equation

$$i\hbar \partial_t |\Psi'(t)\rangle = H'(t) |\Psi'(t)\rangle, \quad (7)$$

where the transformed state is

$$|\Psi'(t)\rangle = e^{\Lambda(t)} |\Psi(t)\rangle, \quad (8)$$

and the Hamiltonian reads

$$H'(t) = e^{\Lambda(t)} H e^{-\Lambda(t)} + i\hbar \frac{\partial}{\partial t} \Lambda(t). \quad (9)$$

Using Eqs. (6) and (9), ignoring constant terms and terms depending only on time, the Hamiltonian $H'(t)$ can be expressed as

$$\begin{aligned} H'(t) = & \hbar\omega A^\dagger A + \hbar\omega \sum_{n=2}^N n a_n^\dagger a_n \\ & + \hbar \sum_{n=2}^N \chi_n \left[a_n^\dagger \sum_{k=1}^n \binom{n}{k} A^k \alpha_0^{n-k} e^{-i(n-k)\omega t} \right. \\ & \left. + a_n \sum_{k=1}^n \binom{n}{k} A^{\dagger k} \alpha_0^{*(n-k)} e^{i(n-k)\omega t} \right] \\ & + \hbar \sum_{n=2}^N \chi_n^2 t \left[i\alpha_0^{*n} \sum_{k=0}^n \binom{n}{k} A^k \alpha_0^{n-k} e^{ik\omega t} \right. \\ & \left. - i\alpha_0^n \sum_{k=0}^n \binom{n}{k} A^{\dagger k} \alpha_0^{*(n-k)} e^{-ik\omega t} \right]. \quad (10) \end{aligned}$$

The transformed Hamiltonian in Eq. (10) can be compartmentalized into terms with distinct physical meanings:

$$H'(t) = H'_F + H'_{DH}(t) + H'_D(t). \quad (11)$$

The first term, $H'_F = \hbar\omega A^\dagger A + \hbar\omega \sum_{n=2}^N n a_n^\dagger a_n$ governs the free evolution of the driving and harmonic field modes. The second Hamiltonian $H'_{DH}(t)$ term, that is the third term in Eq. (10), describes the interaction between the pump and harmonic modes, and is proportional to the first power of the susceptibilities χ_n . The

Hamiltonian $H'_D(t)$, that is, the fourth term in Eq. (10), contributes solely to the evolution of the quantum state of the excitation mode, and is proportional to the second power of susceptibilities χ_n^2 .

To calculate the dynamics of the system, it is practical to use the interaction picture, with the interaction Hamiltonian term being

$$W'(t) = H'_{DH}(t) + H'_D(t). \quad (12)$$

In this picture, the time-evolution of the quantum state $|\Psi'_1(t)\rangle$ is determined by the equation

$$i\hbar \frac{\partial}{\partial t} |\Psi'_1(t)\rangle = e^{iH'_F(t)t} W'(t) e^{-iH'_F(t)t} |\Psi'_1(t)\rangle. \quad (13)$$

The solution of the equation can be written in the general form

$$|\Psi'_1(t)\rangle = \sum_{\mathcal{F}} C_{J,j_2,\dots,j_N}(t) e^{iH'_F t} |J, j_2, \dots, j_N\rangle, \quad (14)$$

where the summation is over the Fock-space under consideration, and $|J, j_2, \dots, j_N\rangle = |J\rangle \otimes \prod_{n=2}^N |j_n\rangle_n$. Here $|J\rangle$ and $|j_n\rangle_n$ are the Fock-states of the driving field mode and the n th harmonic modes, respectively. After inserting Eq. (14) in Eq. (13), the calculations lead to the dynamical equations that govern the coefficients, and can be expressed as

$$i\hbar \dot{C}_{J',j'_2,\dots,j'_N}(t) = C_{J,j_2,\dots,j_N}(t) e^{i\frac{E'-E}{\hbar}t} \\ \times \sum_{\mathcal{F}} \langle J', j'_2, \dots, j'_N | W'(t) | J, j_2, \dots, j_N \rangle, \quad (15)$$

where

$$E \equiv \hbar\omega \left[J + \sum_{n=2}^N n j_n \right], \quad E' \equiv \hbar\omega \left[J' + \sum_{n=2}^N n j'_n \right]. \quad (16)$$

In the following sections, we will analyze these dynamical equations perturbatively.

IV. PERTURBATIVE SOLUTION

In this section, we express the leading-order perturbations in the quantum state of the electromagnetic field. We will consider the initial condition

$$|\Psi'_1(0)\rangle = |0\rangle \otimes |0 \dots 0\rangle, \quad (17)$$

corresponding to $C_{0,0,\dots,0}^{(0)} = 1$ coefficient in Eq. (15). In order to express the quantum state in a transparent way, it is beneficial to rearrange the summations in $W'(t)$, appearing in Eq. (10), before proceeding to solve Eq. (15). Utilizing the identity

$$\sum_{n=2}^N \sum_{k=1}^n f(k, n) = \sum_{k=1}^N \sum_{n=\max\{2,k\}}^N f(k, n), \quad (18)$$

one can express $W'(t)$ as

$$W'(t) = \hbar \sum_{k=1}^N \sum_{n=\max\{2,k\}}^N \chi_n \left[\binom{n}{k} \alpha_0^{n-k} e^{-i(n-k)\omega t} a_n^\dagger A^k \right. \\ \left. + \binom{n}{k} \alpha_0^{*(n-k)} e^{i(n-k)\omega t} a_n A^{\dagger k} \right] \\ + \hbar \sum_{k=0}^N \sum_{n=\max\{2,k\}}^N \chi_n^2 t \left[i \alpha_0^{*n} \binom{n}{k} \alpha_0^{n-k} e^{ik\omega t} A^k \right. \\ \left. - i \alpha_0^n \binom{n}{k} \alpha_0^{*(n-k)} e^{-ik\omega t} A^{\dagger k} \right]. \quad (19)$$

Exploiting $A|0, 0 \dots 0\rangle = 0$ and $a_n|0, 0 \dots 0\rangle = 0$, it is easy to see that the only non-disappearing terms in the first-order iteration of Eq. (15) are

$$\langle J, j_1, \dots, j_N | W'(t) | 0, 0, \dots, 0 \rangle = \\ i\hbar \langle J, j_1, \dots, j_N | \left[\sum_{n=2}^N \chi_n^2 t \alpha_0^{*n} \alpha_0^n | 0, 0, \dots, 0 \rangle \right. \\ \left. - \sum_{k=0}^N \sum_{n=\max\{2,k\}}^N \chi_n^2 t e^{-ik\omega t} \binom{n}{k} \alpha_0^n \alpha_0^{*(n-k)} \sqrt{k!} | k, 0 \dots \rangle \right]. \quad (20)$$

It follows that only the coefficients with $J = k > 0$, $j_2 = \dots = j_N = 0$ indices can be nonzero. Expressing the above equation in an equivalent, but more transparent way, we get

$$\langle k, 0, \dots, 0 | W'(t) | 0, 0, \dots, 0 \rangle = \\ i\hbar \sum_{n=\max\{2,k\}}^N \chi_n^2 t \left[|\alpha_0|^{2n} \delta_{k,0} - \alpha_0^n \binom{n}{k} \sqrt{k!} \alpha_0^{*(n-k)} e^{-ik\omega t} \right]. \quad (21)$$

The first-order contributions can be thus expressed by

$$\dot{C}_{k,0,\dots,0}^{(1)}(t) = \sum_{n=\max\{2,k\}}^N \chi_n^2 t \left[(\delta_{k,0} - 1) \alpha_0^n \binom{n}{k} \sqrt{k!} \alpha_0^{*(n-k)} \right], \quad (22)$$

the integration of which is straightforward, resulting in

$$C_{k,0,\dots,0}^{(1)}(t) = - \sum_{n=\max\{2,k\}}^N \frac{\chi_n^2 t^2 \alpha_0^n}{2} \binom{n}{k} \alpha_0^{*(n-k)} \sqrt{k!} \quad (23)$$

for $k \geq 1$ values. Hence, in first-order iteration, the non-normalized quantum state is written as

$$|\Psi'(t)\rangle^{(1)} = |0\rangle \otimes |0 \dots \rangle - \sum_{k=1}^N \Theta_k t^2 |k\rangle \otimes |0 \dots \rangle, \quad (24)$$

where

$$\Theta_k = \sum_{n=\max\{2,k\}}^N \binom{n}{k} \frac{\chi_n^2 |\alpha_0|^{2n} \sqrt{k!}}{2 \alpha_0^{*k}}. \quad (25)$$

The physical interpretation associated with the first-order iteration is the change of the quantum state of the excitation mode due to back-action described by our model. The perturbative terms in the quantum state represented by Eq. (24) are proportional to powers of $\chi_n t$, therefore one may consider these to be the perturbative parameters. It follows that our results are only valid for small $\chi_n t$ values.

In the second-order iteration, starting from Eq. (24), one must evaluate the matrix elements $\langle J, j_2, \dots, j_N | W'(t) | j, 0, \dots, 0 \rangle$ for $j \neq 0$ values. Note that the terms in Eq. (19) containing $a_n A^{\dagger k}$ give no contribution, since $a_n A^{\dagger k} | j, 0, \dots, 0 \rangle = 0$. Considering the previous procedure, it can be foreseen that the terms proportional to χ_n^2 in Eq. (19) result in contributions of magnitude $\mathcal{O}(\chi_n^4 t^4)$. Consequently, up to the precision of $\mathcal{O}(\chi_n^3 t^3)$, the only non-disappearing terms are

$$\begin{aligned} & \langle J, j_2, \dots, j_N | W'(t) | j, 0, \dots, 0 \rangle = \\ & \langle J, j_1, \dots, j_N | \sum_{k=1}^N \hbar \sum_{n=\max[2,k]}^N \chi_n \binom{n}{k} \alpha_0^{n-k} e^{-i(n-k)\omega t} \\ & \quad \times a_n^\dagger A^k | j, 0, \dots, 0 \rangle. \end{aligned} \quad (26)$$

It follows that the only non-negligible contribution is for indices $J = j - k$, $j_n = 1$, and $\forall q \neq n : j_q = 0$. Finally, we obtain the dynamical equations for the second-order iteration as

$$\begin{aligned} i\hbar \dot{C}_{k', 0, \dots, 1, n', \dots, 0}^{(2)} &= \sum_{j=1}^N \sum_{k=1}^N \hbar \sum_{n=\max[2,k]}^N \chi_n \binom{n}{k} \alpha_0^{n-k} \\ & \times e^{-i(n-k)\omega t} \underbrace{\sqrt{\frac{j!}{j-k!}} \langle k' | j - k \rangle}_{\delta_{k', j-k}} \underbrace{\langle n' | 1 | 1 \rangle_n}_{\delta_{n', n}} \Theta_j t^2 e^{i(k'+n'-j)\omega t}. \end{aligned} \quad (27)$$

After some simplification, one can write

$$\dot{C}_{k', 0, \dots, 1, n', \dots, 0}^{(2)}(t) = -i \sum_{k=1}^N \chi_{n'} \binom{n'}{k} \alpha_0^{n'-k} \sqrt{\frac{k+k'}{k!}} \Theta_{k+k'} t^2, \quad (28)$$

where the expression $\binom{n'}{k} = 0$ if $k > n'$. The solution of Eq. (27) is straightforward, and we write

$$C_{k', \dots, 0, 1, n', \dots, 0}^{(2)}(t) = -i \Omega_{n', k'} t^3, \quad (29)$$

where

$$\Omega_{n', k'} = \sum_{k=1}^N \chi_{n'} \binom{n'}{k} \alpha_0^{n'-k} \sqrt{\frac{(k+k')!}{k!}} \frac{\Theta_{k+k'}}{3}. \quad (30)$$

The physical interpretation associated with the second-order iteration is a multitude of simultaneous modifications of the quantum state of the driving field and of one harmonic mode.

Finally, the quantum state after the second-order iteration can be written as

$$\begin{aligned} |\Psi'(t)\rangle^{(2)} &= |0\rangle \otimes \prod_{n=2}^N |0\rangle_n - \sum_{k=1}^N \Theta_k t^2 |k\rangle \otimes \prod_{n=2}^N |0\rangle_n e^{-ik\omega t} \\ & - i \sum_{k=0}^N \sum_{j=2}^N \Omega_{j,k} t^3 |k\rangle \otimes \prod_{\substack{n=2 \\ n \neq j}}^N |0\rangle_n \otimes |1\rangle_j e^{-i(k+j)\omega t}. \end{aligned} \quad (31)$$

To illustrate the emerging entanglement between the harmonics, we specifically consider the case of $N = 3$, that reads

$$\begin{aligned} |\Psi'(t)\rangle &= \left(|0\rangle - \sum_{k=1}^3 \Theta_k t^2 e^{-ik\omega t} |k\rangle \right) \otimes |0\rangle_2 |0\rangle_3 \\ & - i \sum_{k=0}^3 \Omega_{2,k} t^3 e^{-i(k+2)\omega t} |k\rangle \otimes |1\rangle_2 |0\rangle_3 \\ & - i \sum_{k=0}^3 \Omega_{3,k} t^3 e^{-i(k+3)\omega t} |k\rangle \otimes |0\rangle_2 |1\rangle_3. \end{aligned} \quad (32)$$

Here, one can observe that a Bell-state-like correlation appears between the harmonic modes.

For the sake of completeness, we derive the original $|\Psi(t)\rangle$ quantum state by inverting the transformations of Eq. (8) which results in

$$\begin{aligned} |\Psi(t)\rangle &= |\alpha_0 e^{-i\omega t}\rangle \otimes \prod_{n=2}^N | -it\chi_n \alpha_0^n e^{-in\omega t} \rangle_n \\ & - \sum_{k=1}^N \Theta_k t^2 |\alpha_0 e^{-i\omega t}, k\rangle \otimes \prod_{n=2}^N | -it\chi_n \alpha_0^n e^{-in\omega t} \rangle_n e^{-ik\omega t} \\ & - i \sum_{k=0}^N \sum_{j=n_1}^N \Omega_{j,k} t^3 |\alpha_0 e^{-i\omega t}, k\rangle \otimes \prod_{\substack{n=2 \\ n \neq j}}^N | -it\chi_n \alpha_0^n e^{-in\omega t} \rangle_n \\ & \quad \otimes | -it\chi_j \alpha_0^j e^{-ij\omega t}, 1 \rangle_j e^{-i(k+j)\omega t}. \end{aligned} \quad (33)$$

Accordingly, the resulting quantum state of the exciting and harmonic modes is an entangled superposition state in the displaced number-state basis. Based on these considerations, it is clear that second-order iteration is needed to reveal intermodal correlations.

Note that both the harmonics and the driving field become slightly non-Gaussian as a result of the interaction. To show the deviation from coherent states, we calculate the leading term difference arising in the Wigner-function [99] of the density-matrix associated with the n th harmonic mode. After construction of the density matrix [see App.B for details] and tracing out all but one

harmonic mode, we get

$$\begin{aligned}
\rho_{n'th}^{(2)}(t) &= \sum_{k=0}^N |\Omega_{n,k}|^2 t^6 |1\rangle_n \langle 1|_n \\
&+ \left[1 + \sum_{k=1}^N |\Theta_k|^2 t^4 + \sum_{k=0}^N \sum_{j=n_1, j \neq n}^N |\Omega_{j,k}|^2 t^6 \right] |0\rangle_n \langle 0|_n \\
&+ it^3 \left[\Omega_{n,0}^* e^{in\omega t} |0\rangle_n \langle 1|_n - \Omega_{n,0} e^{-in\omega t} |1\rangle_n \langle 0|_n \right] \\
&- it^5 \sum_{k=1}^N \left[\Theta_k \Omega_{n,k}^* e^{in\omega t} |0\rangle_n \langle 1|_n - \Theta_k^* \Omega_{n,k} e^{-in\omega t} |1\rangle_n \langle 0|_n \right].
\end{aligned} \tag{34}$$

We have calculated the deviation from coherent states through $\frac{\rho_{n'th}^{(2)}(t)}{\text{Tr}[\rho_{n'th}^{(2)}(t)]} - |0\rangle_n \langle 0|_n$, which is shown on Fig. 1. Note that the unitary transformation connecting ρ and ρ' is merely a displacement. The deviation is small, and would not be visible on plots of $\frac{\rho_{n'th}^{(2)}(t)}{\text{Tr}[\rho_{n'th}^{(2)}(t)]}$ itself.

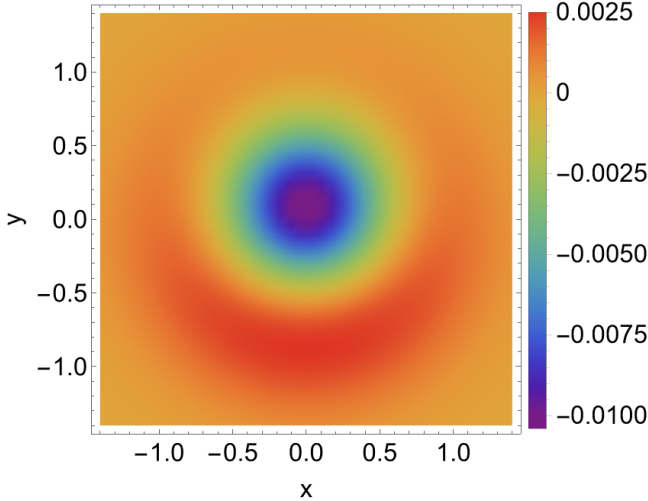


FIG. 1. Deviation in the Wigner function of the 10th harmonic, $\frac{\rho_{10}^{(2)}(t)}{\text{Tr}[\rho_{10}^{(2)}(t)]} - |0\rangle_{10} \langle 0|_{10}$, based on [Eq. (34)], for driving pulse of 2 optical cycles. Parameters are chosen as $|\alpha_0| = 10^2$, $t = 2\frac{2\pi}{\omega}$ and $\chi_n = \frac{1}{\sqrt{n}|\alpha_0|^n}$, with harmonic orders being in $n \in 3, \dots, 10$.

Next, we calculate the quantities that we intend to use for analysis in the next section. Using the quantum state given by Eq. (33), we present the full analytical formulae in App.A. Here, without loss of generality, we use the special initial condition $\alpha_0 = -i|\alpha_0|$, which simplifies

the formulae. With this, we get

$$\begin{aligned}
\Theta_k &= (-i)^k |\Theta_k| \\
|\Theta_k| &= \sum_{n=\max\{2,k\}}^N \binom{n}{k} \frac{\sqrt{k!}}{2} \chi_n^2 |\alpha_0|^{2n-k}, \\
\Omega_{n',k'} &= (-i)^{n'+k'} |\Omega_{n',k'}| \\
|\Omega_{n',k'}| &= \sum_{k=1}^N \frac{|\chi_{n'}|}{3} \binom{n'}{k} \sqrt{\frac{(k+k')!}{k'!}} |\alpha_0|^{n'-k} |\Theta_{k+k'}|.
\end{aligned} \tag{35}$$

$$\tag{36}$$

With these parameters, the quantum state can be evaluated, and calculations of one-time operator mean-values can be done in a lengthy, but straightforward manner.

Recall that $|\Psi(t)\rangle$ is a perturbatively calculated state, accordingly, it is not normalized. For the purpose of expressing any physical quantities, first we need to calculate the square of the norm $\mathcal{N}(t) = \langle \Psi(t) | \Psi(t) \rangle$, that is

$$\mathcal{N}(t) = 1 + \sum_{k=1}^N |\Theta_k|^2 t^4 + \sum_{k=0}^N \sum_{j=2}^N |\Omega_{j,k}|^2 t^6. \tag{37}$$

One of the most fundamental quantity for our analysis is the mean photon-number of the modes. For the excitation mode, it is $\langle N_1(t) \rangle = \frac{1}{\mathcal{N}(t)} \langle \Psi(t) | A^\dagger A | \Psi(t) \rangle$, and for the n th harmonic mode, the mean photon-number is $\langle N_n(t) \rangle = \frac{1}{\mathcal{N}(t)} \langle \Psi(t) | a_n^\dagger(t) a_n(t) | \Psi(t) \rangle$, respectively:

$$\begin{aligned}
\langle N_1(t) \rangle &= |\alpha_0|^2 + \frac{1}{\mathcal{N}(t)} \left[-2|\Theta_1| |\alpha_0|^2 \right. \\
&+ \sum_{k=1}^N \left(k |\Theta_k|^2 + 2\sqrt{k+1} |\alpha_0| |\Theta_k| |\Theta_{k+1}| \right) t^4 + \\
&\left. \sum_{k=0}^N \sum_{j=2}^N \left(k |\Omega_{j,k}|^2 + 2\sqrt{k+1} |\alpha_0| |\Omega_{j,k}| |\Omega_{j,k+1}| \right) t^6 \right], \tag{38}
\end{aligned}$$

$$\begin{aligned}
\langle N_n(t) \rangle &= \chi_n^2 |\alpha_0|^{2n} t^2 + \frac{1}{\mathcal{N}(t)} \left[2\chi_n |\alpha_0|^n |\Omega_{n,0}| t^4 \right. \\
&+ \left. \left(\sum_{k=0}^N |\Omega_{n,k}|^2 - 2\chi_n \sum_{k=1}^N |\alpha_0|^n |\Theta_k| |\Omega_{n,k}| \right) t^6 \right]. \tag{39}
\end{aligned}$$

To analyze quantum properties of any particular mode, we will utilize the second-order one-time photon coherence functions G_{nm} , particularly as part of other, composite quantities. To characterize the driving field mode, we use $G_{11}(t) = \frac{1}{\mathcal{N}(t)} \langle \Psi(t) | A^\dagger A^\dagger A A | \Psi(t) \rangle$, which reads as

$$\begin{aligned}
G_{11}(t) = & |\alpha_0|^4 + \frac{1}{\mathcal{N}(t)} \left[-2\sqrt{2}|\alpha_0|^2(|\Theta_2| + \sqrt{2}|\alpha_0||\Theta_1|)t^2 \right. \\
& + \sum_{k=1}^N |\Theta_k| \left(|\Theta_k|(k(k-1+4|\alpha_0|^2)) + 4|\alpha_0|^3\sqrt{k+1}|\Theta_{k+1}| \right) t^4 \\
& + 4 \sum_{k=0}^N k\sqrt{k+1}|\alpha_0||\Theta_k||\Theta_{k+1}|t^4 \\
& + 2 \sum_{k=1}^N \sqrt{k+1}\sqrt{k+2}|\alpha_0|^2|\Theta_k||\Theta_{k+2}|t^4 \\
& + \sum_{k=0}^N \sum_{j=2}^N |\Omega_{j,k}|^2 [k(k-1) + 4|\alpha_0|^2k] t^6 \\
& + 4|\alpha_0|^3 \sum_{k=0}^N \sum_{j=2}^N \sqrt{k+1}|\Omega_{j,k}||\Omega_{j,k+1}|t^6 \\
& + 2 \sum_{k=0}^N \sum_{j=2}^N \sqrt{k+1}\sqrt{k+2}|\alpha_0|^2|\Omega_{j,k}||\Omega_{j,k+2}|t^6 \\
& \left. + 4 \sum_{k=0}^N \sum_{j=2}^N k\sqrt{k+1}|\alpha_0||\Omega_{j,k+1}||\Omega_{j,k}|t^6 \right], \tag{40}
\end{aligned}$$

while for the n th ($n \neq 1$) harmonic mode, we use $G_{nn}(t) = \frac{1}{\mathcal{N}(t)} \langle \Psi(t) | a_n^\dagger a_n^\dagger a_n a_n | \Psi(t) \rangle$, which we express as

$$\begin{aligned}
G_{nn}(t) \approx & \chi_n^4 |\alpha_0|^{4n} t^4 + \frac{1}{\mathcal{N}(t)} \left[4\chi_n^3 |\alpha_0|^{3n} |\Omega_{n,0}| t^6 + \right. \\
& \left. \left(4\chi_n^2 |\alpha_0|^{2n} \sum_{k=0}^N |\Omega_{n,k}|^2 - 4\chi_n^3 |\alpha_0|^{3n} \sum_{k=1}^N |\Omega_{n,k}||\Theta_k| \right) t^8 \right]. \tag{41}
\end{aligned}$$

With these quantities given, we can proceed to calculate the second-order normalized photon correlation functions γ_{nm} , which are often the primary experimentally measured quantities involving nonclassical photon states. The correlations of the excitation and harmonic modes are $\gamma_{11}(t) = \frac{G_{11}(t)}{\langle N_1(t) \rangle \langle N_1(t) \rangle}$ and $\gamma_{nn}(t) = \frac{G_{nn}(t)}{\langle N_n(t) \rangle \langle N_n(t) \rangle}$, respectively. These autocorrelation functions can be used to characterize the photon statistics of single modes, e.g. revealing super- or sub-Poissonian distributions.

Turning our attention to the rich structure inherent in many-mode states, the fundamental tools we use to gain insight are the second-order one-time intermodal cross-coherence functions. The coherence between the pump mode and the n th ($n \neq 1$) harmonic mode is $G_{1n}(t) = \frac{1}{\mathcal{N}(t)} \langle \Psi(t) | A^\dagger a_n^\dagger a_n A | \Psi(t) \rangle$, written as

$$\begin{aligned}
G_{1n}(t) \approx & \chi_n^2 |\alpha_0|^{2n+2} t^2 + \frac{1}{\mathcal{N}(t)} \left[-2\chi_n^2 |\alpha_0|^{2n+1} |\Theta_1| t^4 \right. \\
& + 2\chi_n |\alpha_0|^{n+2} \left(|\Omega_{n,0}| t^4 - \sum_{k=1}^N |\Theta_k||\Omega_{n,k}| t^6 \right) \\
& + 2\chi_n |\alpha_0|^{(n+1)} \left(|\Omega_{n,1}| t^4 - \sum_{k=2}^N \sqrt{k} |\Theta_{k-1}||\Omega_{n,k}| t^6 \right) \\
& + \sum_{k=0}^N |\Omega_{n,k}|^2 (k + |\alpha_0|^2) t^6 - 2\chi_n |\alpha_0|^n \sum_{k=1}^N k |\Theta_k||\Omega_{n,k}| t^6 \\
& + 2 \sum_{k=0}^N \sqrt{k+1} |\alpha_0||\Omega_{n,k}||\Omega_{n,k+1}| t^6 \\
& + \chi_n^2 |\alpha_0|^{2n} \left(\sum_{k=1}^N k |\Theta_k|^2 t^6 + \sum_{k=0}^N \sum_{j=2}^N k |\Omega_{j,k}|^2 t^8 \right) \\
& - 2\chi_n |\alpha_0|^{n+1} \sum_{k=0}^N \sqrt{k+1} |\Theta_{k+1}||\Omega_{n,k}| t^6 \\
& + 2\chi_n^2 |\alpha_0|^{2n+1} \left(\sum_{k=1}^N \sqrt{k+1} |\Theta_k||\Theta_{k+1}| t^6 \right. \\
& \left. + \sum_{k=0}^N \sum_{j=2}^N \sqrt{k+1} |\Omega_{j,k}||\Omega_{j,k+1}| t^8 \right) \Big], \tag{42}
\end{aligned}$$

while between the n th ($n \neq 1$) and m th ($m \neq n$) harmonic modes, it is $G_{nm}(t) = \frac{1}{\mathcal{N}(t)} \langle \Psi(t) | a_m^\dagger a_n^\dagger a_n a_m | \Psi(t) \rangle$, which reads

$$\begin{aligned}
G_{nm}(t) \approx & \chi_n^2 \chi_m^2 |\alpha_0|^{2n+2m} t^4 + \\
& \frac{1}{\mathcal{N}(t)} \left[2 \left(\chi_n \chi_m^2 |\alpha_0|^{2m+n} |\Omega_{n,0}| + \chi_n^2 \chi_m |\alpha_0|^{2n+m} |\Omega_{m,0}| \right) t^6 \right. \\
& + 2\chi_n \chi_m |\alpha_0|^{n+m} \sum_{k=0}^N |\Omega_{m,k}||\Omega_{n,k}| t^8 \\
& + \sum_{k=0}^N \left(|\Omega_{n,k}|^2 \chi_m^2 |\alpha_0|^{2m} + |\Omega_{m,k}|^2 \chi_n^2 |\alpha_0|^{2n} \right) t^8 \\
& - 2\chi_n \chi_m^2 |\alpha_0|^{2m+n} \sum_{k=1}^N |\Omega_{n,k}||\Theta_k| t^8 \\
& \left. - 2\chi_m \chi_n^2 |\alpha_0|^{2n+m} \sum_{k=1}^N |\Omega_{m,k}||\Theta_k| t^8 \right]. \tag{43}
\end{aligned}$$

From these, we can construct the experimentally measurable intermodal photon correlation functions. The correlation between the excitation and n th harmonic modes is $\gamma_{1n}(t) = \frac{G_{1n}(t)}{\langle N_1(t) \rangle \langle N_n(t) \rangle}$, while between n th and m th order harmonics is $\gamma_{nm}(t) = \frac{G_{nm}(t)}{\langle N_n(t) \rangle \langle N_m(t) \rangle}$, respectively. Of special interest to us is the $R(t)$ function defined as

$$R(t) = \frac{\gamma_{nm}^2(t)}{\gamma_{nn}(t)\gamma_{mm}(t)} = \frac{G_{nm}^2(t)}{G_{nn}(t)G_{mm}(t)}, \tag{44}$$

which have been measured in Ref. [1], and found to have values $R > 1$. This violates the CBS-inequality (Cauchy-Bunyakovsky-Schwarz inequality), and hence implies nonclassical correlation in the quantum state of the considered modes [100, 101]. One relevant theoretical calculation, involving atomic HHG, can be found in Ref. [64].

We are especially interested in the presence of entanglement, which, of course, is a nonclassicality itself, but is not necessarily implied by $R > 1$ relation. To measure intermodal entanglement between harmonics, we use the logarithmic negativity, applied to $\rho_{nm}^{\prime(2)}$ density-matrix, wherein we traced out all but two modes, corresponding to the n th and m th harmonics.

$$E_{nm}(t) = \log_2 \left\| \left(\frac{1}{\text{Tr}[\rho_{nm}^{\prime(2)}(t)]} \rho_{nm}^{\prime(2)}(t) \right)^{\Gamma_n} \right\|_1 \quad (45)$$

When calculating Eq. (45), we use $(\rho_{nm}^{\prime(2)})^{\Gamma_n}$ derived in App.B with the result expressed in Eq. (B5), specifically.

V. INTERPRETATION OF THE RESULTS

In this section, we analyze how our model can account for experimentally measurable effects. The considerations laid down in the previous section leave the amplitude $|\alpha_0|$, the interaction time, or temporal pulse duration, $t = \tau$, the cutoff-order N , and susceptibilities $\{\chi_n\}$ as free parameters. For modeling a given experiment, the parameters $(|\alpha_0|, \tau, N)$ can be chosen according to the experimentally measured values.

The χ_n susceptibilities are not directly measurable, therefore we fit their values based on physical considerations. The measured energy spectrum of the harmonics $\{I_n(|\alpha_0|, \tau)\} = \{\hbar\omega_n \langle N_n(|\alpha_0|, \tau) \rangle\}$ induced by a driving pulse of amplitude $|\alpha_0| = \sqrt{\epsilon_0 V / 2\hbar\omega E_0}$ and temporal duration τ , can be used to determine χ_n . Assuming that the zeroth-order approximation [Eq. (2)] acceptably predicts the harmonic energy spectrum, one can write

$$I_n(|\alpha_0|, \tau) = |\alpha_0|^{2n} \chi_n^2(|\alpha_0|) \hbar\omega_n \tau^2, \quad (46)$$

where we explicitly denoted the potential amplitude-dependence of the susceptibilities. Then χ_n can be expressed through experimentally measurable spectrum as

$$\chi_n(|\alpha_0|) = \sqrt{\frac{I_n(|\alpha_0|, \tau)}{|\alpha_0|^{2n} \hbar\omega_n \tau^2}}. \quad (47)$$

We note that for analysis, one can choose some parameters freely, utilizing the scaling relations rooted in Eq. (46). First, it follows that one can always scale up interaction time τ with the transformation

$$(\chi_n, \tau) \rightarrow (\frac{1}{\xi} \chi_n, \xi \tau). \quad (48)$$

Similarly, for a given harmonic energy I_n and fixed interaction time τ , only the product $|\alpha_0|^{2n} \chi_n^2$ needs to be invariant. Hence, one can choose arbitrary coherent amplitude α_0 with corresponding susceptibilities χ_n , according to the transformation

$$(\alpha_0, \chi_n \tau) \rightarrow (\xi \alpha_0, \frac{1}{|\xi|^n} \chi_n \tau). \quad (49)$$

We note that the τ parameter can be eliminated by considering χ_n/χ_m ratios, since

$$\frac{\chi_n(|\alpha_0|)}{\chi_m(|\alpha_0|)} = \sqrt{\frac{I_n(|\alpha_0|, \tau) m}{I_m(|\alpha_0|, \tau) n}} \frac{|\alpha_0|^m}{|\alpha_0|^n}. \quad (50)$$

In realizations of HHG, odd-order harmonics often dominate the spectrum, that is, $\chi_n \neq 0$ only when n is an odd natural number. We stress that the "only-odd-harmonics" rule is strictly only valid for material targets with inversion symmetry, together with monochromatic excitation, for example atomic gases driven by quasi-monochromatic pulses [102]. We will accept this assumption as valid in the following, but we emphasize that it can be abandoned without loss of generality.

There are two aspects of the harmonic spectrum that are commonly used to categorize qualitative features of HHG: how the decrease of the harmonic energies depends on the increasing harmonic order, and the dependence of individual harmonic energies on the driving pulse amplitude. The literature of HHG distinguishes between the so-called perturbative regime and the nonperturbative regime. The idea behind the concept of perturbative regime is that the harmonic energies $\{I_n\}$ in this regime scale with the laser pulse energy I_0 as $\propto I_0^n$ for low pump intensities, which behaviour is characteristic of perturbative processes. On the contrary, the spectrum in the nonperturbative regime deviates from the scaling characterizing the perturbative regime, and for sufficiently high intensity driving, generally characterized by a plateau-like harmonic spectrum. Subsequently, we show how our model can be applied in both regimes. Then we examine how the model can be fitted to the experimental data measured in Ref. [1].

A. Perturbative regime

The perturbative regime, physically corresponding to low driving intensities, is characterized by the domination of the lower-order harmonics. There are two defining features: First, harmonic energies fall off exponentially with increasing order of harmonics. We note that at very high orders the decrease can even be inverse factorial [103]. The exponential decrease can be expressed as $I_n \propto C p^{2n}$, where $p \in [0, 1)$ and $C \in \mathbf{R}^+$. Second, the harmonic energies scale with the driving amplitude as $I_n \propto |\alpha_0|^{2n}$. These two conditions together lead to

$$I_n(|\alpha_0|, \tau) = \frac{\hbar\omega_n}{n} C p^{2n} |\alpha_0|^{2n} \tau^2, \quad (51)$$

from which, using Eq. (47), we can express susceptibilities as

$$\chi_n(|\alpha_0|) = \sqrt{\frac{C}{n}} p^n. \quad (52)$$

Accordingly, the properly determined susceptibilities in our model are independent of the driving pulse energy in the perturbative regime.

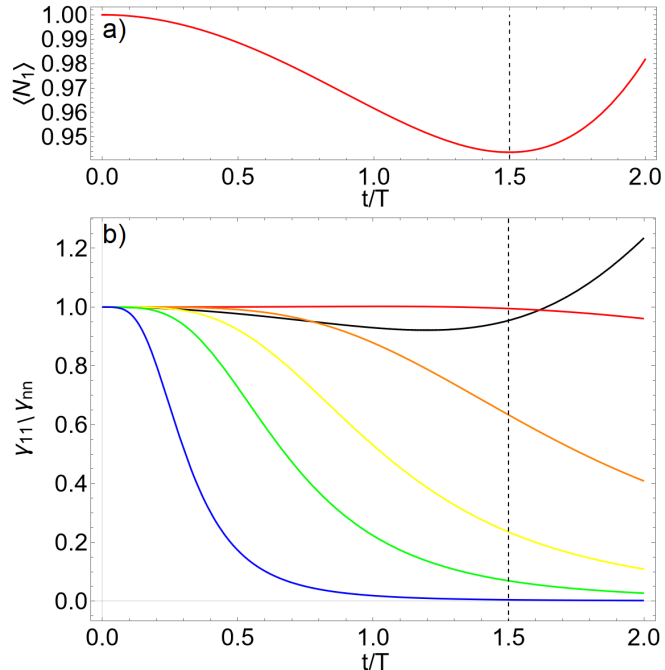


FIG. 2. Single-mode physical quantities characterizing the excitation and harmonics. a) Time-evolution of $\langle N_1(t) \rangle$ shown as a function of t/T , where $T = 2\pi/\omega$ is the optical cycle. b) Time-evolution of the photon correlations: $\gamma_{1,1}(t)$ (black), $\gamma_{3,3}$ (red); $\gamma_{5,5}(t)$ (orange); $\gamma_{7,7}(t)$ (yellow); $\gamma_{9,9}(t)$ (green); $\gamma_{11,11}(t)$ (blue). The parameters are chosen such that $|\alpha_0| = 1$, $\chi_3 = 0.02$, $p = 0.3$, with a cutoff order of $N = 11$. Dashed lines show the chosen interaction time $t = 1.5T$, applied in Fig. (3)

Figure 2 shows the physical quantities characterizing the excitation mode and harmonic modes, introduced in the second half of the previous section. The parameters are chosen such that the amplitude is $|\alpha_0| = 1$, and $\chi_3 = 0.02$, $p = 0.3$, with a cutoff order of $N = 11$. Fig. 2(a) shows the time-evolution of mean photon value of the excitation mode $\langle N_1(t) \rangle$ given in Eq. (38) as a function of dimensionless time t/T , where $T = 2\pi/\omega$ is the optical cycle of the driving field. The vertical dashed line shows the chosen interaction time of three-half optical cycles $t = 1.5T$, which will be applied to calculate two-mode physical quantities. We note that such a choice practically corresponds to a monochromatic driving pulse with a rectangular carrier envelope. The interaction between the excitation and harmonic modes leads to an initial decrease of $\langle N_1(t) \rangle$, i.e. photon absorption from

the driving mode, which is both intuitive and measurable. On the other hand, the subsequent increase corresponds to an energy transfer from the harmonics into the driving field, which practically cannot be measured experimentally. This phenomenon can pose a limitation for the physical validity of our model.

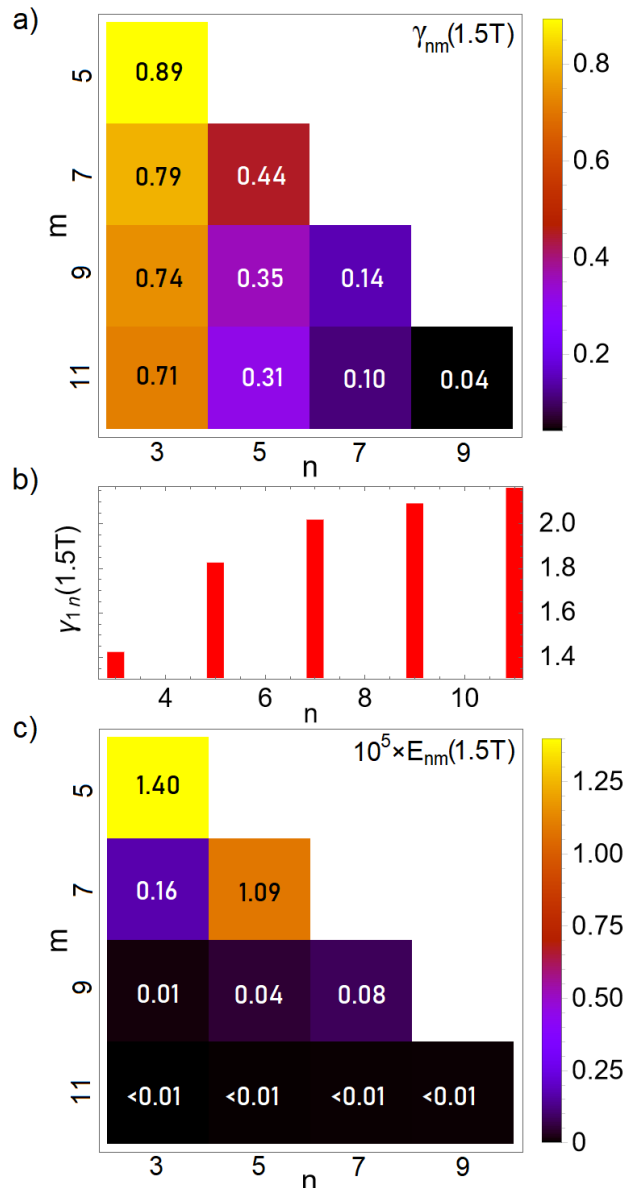


FIG. 3. Two-mode physical quantities. Intermodal correlation function values $\gamma_{nm}(1.5T)$ and $\gamma_{1n}(1.5T)$ a) between harmonic modes and b) between the excitation mode and harmonic modes, respectively. c) Upscaled logarithmic negativity between harmonic modes $10^5 \times E_{nm}(1.5T)$.

The time-evolution of the photon autocorrelations $\gamma_{j,j}$ for the modes $j = 1, 3, \dots, 11$ is presented in Fig. 2(b). Comparing the values of correlation functions for the harmonics, they show a clear tendency of decreasing with both harmonic order and time. Harmonic modes are characterized by sub-Poissonian photon statistics, and

this characteristic is especially significant for higher order harmonics. The correlation function of the pump mode $\gamma_{11}(t)$ has a moderately decreasing tendency with time, but close to the chosen interaction time $t = 1.5T$, it starts increasing, representing a super-Poissonian statistics.

The two-mode physical quantities are shown on Fig. 3, calculated with identical parameters as were used for the single-mode quantities. Inter-harmonic correlation values at the end of the interaction $\gamma_{nm}(1.5T)$ are plotted in Fig. 3(a). These are generally of lower than unit value, and the qualitative tendency is that correlation is larger if at least one harmonic is of lower order. Fig. 3(b) presents the intermodal correlation values $\gamma_{1n}(1.5T)$ between the excitation mode and harmonic modes. Cross-correlations between the driving and harmonic modes are positive, which is what one expects for driving and driven modes. It can reach values $\gamma_{1n} > 2$, primarily when the harmonics are of higher order. For high-order harmonic pairs, significant sub-Poissonian photon statistic, that is $\gamma_{nn} < 1$, and simultaneous anti-correlations between these modes, characterized by $\gamma_{nm} < 1$, are present, implying nonclassical quantum properties. To analyze pairwise entanglement, the logarithmic negativity between harmonics, expressed through Eq. (45), are shown on Fig. 3(e), upscaled by a factor of 10^5 . The values quickly decrease as harmonic orders increase. Comparing Fig. 3(a) and Fig. 3(c), one can conclude, that lower-order harmonic pairs have more pronounced entanglement, while higher-order harmonic pairs are associated with more pronounced anti-correlations.

Therefore, nonclassical correlations characterize both lower-order and higher-order pairs of harmonics, however, the exact nature of these nonclassicalities differ. We note here that the calculated value $R_{3,5}(1.5T) \approx 1.2$ (not shown) can fall within the range of measured values for HHG using semiconductor materials in Ref. [1].

B. Idealized nonperturbative regime

The term nonperturbative regime –in the context of HHG– typically refers to setups in which the driving intensity is of higher value. The harmonic energies in the resulting spectrum, after an exponential decrease at the lowest harmonics, reach a plateau-like, nearly constant value. This plateau extends over multiple harmonic orders before reaching a cutoff frequency. The exact structure of the plateau, which can be multi-leveled, varies depending on the material system. Due to the complexities involved, we will consider an idealized version of the nonperturbative regime, in which the harmonic energies are independent of the harmonic order. This leads to: $I_n(|\alpha_0|, \tau) = \frac{\hbar\omega_n}{n} C\tau^2$ and

$$\chi_n(|\alpha_0|) = \sqrt{\frac{C}{n}} \frac{1}{|\alpha_0|^n}, \quad (53)$$

respectively. Unsurprisingly, the properly determined susceptibilities in our model are intensity-dependent in

the nonperturbative regime.

Fig. 4 shows the time-evolution of the photon autocorrelation functions of the excitation mode $\gamma_{11}(t)$ as black; and of the harmonics γ_{nn} as colored curves. The parameters were chosen to be $|\alpha_0| = \sqrt{20}$, and $\chi_3 = 0.0002$, with a cutoff order of $N = 11$. The vertical dashed line shows the chosen interaction time of two optical cycles $t = 2T$, which will be applied to calculate two-mode physical quantities. We note that such a choice practically corresponds to a monochromatic driving pulse with a rectangular carrier envelope. Comparing the values of correlation functions of the harmonics $\gamma_{nn}(t)$, they exhibit slightly super-Poissonian photon statistics, with a clear tendency of initial increase with both time and harmonic order. This dynamics markedly differs from that found in the perturbative regime. The initial increase is followed by a subsequent decrease, which takes place sooner for higher-order harmonics. The correlation function of the excitation mode $\gamma_{11}(t)$ have a moderately increasing tendency with time, representing a slightly super-Poissonian statistics at the chosen interaction time $t = 2T$.

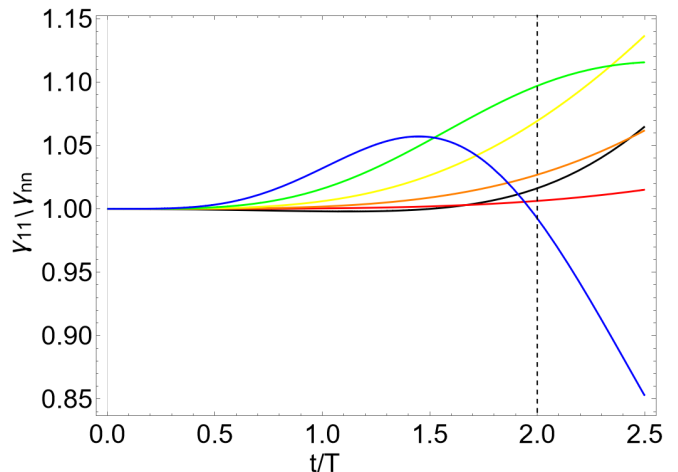


FIG. 4. Time-evolution of the photon correlation functions, shown as a function of t/T , where $T = 2\pi/\omega$ is the optical cycle. $\gamma_{1,1}(t)$ is shown as black, $\gamma_{3,3}$ red; $\gamma_{5,5}(t)$ orange; $\gamma_{7,7}(t)$ yellow; $\gamma_{9,9}(t)$ green; $\gamma_{11,11}(t)$ blue curves. Dashed lines show the corresponding interaction time $t = 2T$. Parameters are $|\alpha_0| = \sqrt{20}$, $\chi_3 = 0.0002$, $N = 11$.

The two-mode physical quantities are displayed on Fig. 5, calculated with identical parameters as used for the single-mode correlations. Inter-harmonic correlation functions $\gamma_{nm}(t)$, evaluated at interaction time $t = 2T$, are plotted in Fig. 3(a). These are generally of slightly above unit value, implying a moderately increased correlation between photon emissions into different harmonic modes. The qualitative tendency is that inter-harmonic correlation is more pronounced between higher-order harmonic pairs. Fig. 3(b) presents the intermodal correlation values between the excitation mode and harmonic modes $\gamma_{1n}(2T)$. These values are positive, but lower than in the perturbative regime. Comparing these two figures,

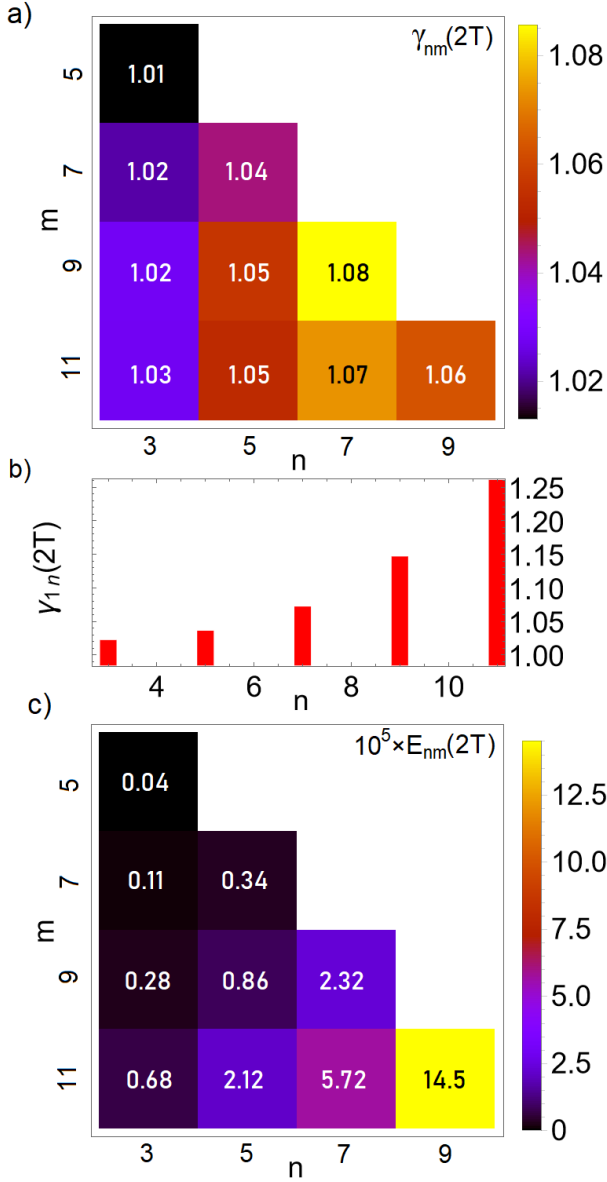


FIG. 5. Two-mode physical quantities. Intermodal correlation function values $\gamma_{nm}(2T)$ and $\gamma_{1n}(2T)$ a) between harmonic modes and b) between the excitation mode and harmonic modes, respectively. c) Upscaled Logarithmic negativity between harmonic modes $10^5 \times E_{nm}(2T)$.

it can be observed that all calculated cross-correlations, both excitation-harmonic and harmonic-harmonic ones have lower values than 2.

To analyze pairwise entanglement, the logarithmic negativity between harmonics, expressed through Eq. (45) have been plotted on Fig. 3(c), scaled up by a factor of 10^5 . One can see that the inter-harmonic entanglement are more pronounced between higher-order harmonics. It can be observed, that entanglement is more pronounced within high-order harmonic pairs.

While we will not delve into potential tripartite (or more general multipartite) entanglement in this study,

we would like to point out that it is possible to find three harmonic modes (a, b, c) within the spectrum that simultaneously exhibit $E_{a,b} > 0$, $E_{a,c} > 0$, and $E_{b,c} > 0$. This indicates that, at least, entanglement between bipartite reductions is present.

C. Fitting to experimental results

Now we turn our attention to an analysis of the experimental measurements reported in Ref. [1]. In this experiment, a pulse of intermediate intensity was used, and the 3rd and 5th order harmonics were studied for GaAs, ZnO and Si targets. Photons-per-pulse associated with these modes, as well as their auto-; and cross-correlation functions γ_{33} , γ_{55} and γ_{35} , respectively, have been measured, and R_{35} have been determined. These quantities were examined as functions of the driving intensity $\hbar\omega \frac{|\alpha_0|^2 c}{V}$, where V is the interaction volume. The driving intensity, of course, is proportional to the pulse energy $\hbar\omega |\alpha_0|^2$. The process of harmonic generation within the used range of laser intensities contains both the perturbative regime, and the onset of a low-intensity nonperturbative regime. The transition between these two regimes occur relatively suddenly, around a certain $|\alpha_0| = \alpha(n)$ driving amplitude, which depends on the harmonic order n . The measured harmonic energies scale with the driving amplitude as $I_n \propto |\alpha_0|^{\epsilon_n}$, with exponent $\epsilon_n < 2n$ in the nonperturbative regime.

We fit the susceptibilities through the measured mean photons per pulse in the harmonic modes, using the zeroth order solution Eq. (2), as in the previous subsections, and assume that the laser pulse energy can be written as $I_0 = \hbar\omega |\alpha_0|^2$. Similarly, we express the mean photons per pulse associated with the n th harmonic as $I_n/\hbar\omega_n$. These assumptions are justified by the fact that the measured mean photons are low, corresponding to a low $\chi_n t$ value in Eq. (39). Hence, the leading-order correction in the mean photon-number due to deviation from a coherent state is small. Thus, one can safely approximate the photons per pulse measurements $\frac{I_n}{\hbar\omega} \approx \chi_n^2 \tau^2 |\alpha_0|^2$ to fit the χ_n susceptibilities. Given the scaling $I_n \propto |\alpha_0|^{\epsilon_n}$, we can proceed as

$$\chi_n^2 (|\alpha_0|) \tau^2 |\alpha_0|^{2n} = C_n \tau^2 |\alpha_0|^{\epsilon_n}, \quad (54)$$

$$\langle N_n(\tau) \rangle \approx C_n \tau^2 \left(\frac{I_0}{\hbar\omega} \right)^{\epsilon_n/2}. \quad (55)$$

From Eq. (54) we can derive the susceptibilities as $\chi_n(|\alpha_0|) = \sqrt{C_n/|\alpha_0|^{2n-\epsilon_n}}$. These susceptibilities are, of course, intensity-dependent in the nonperturbative regime, in agreement with the previous subsection. Equation (55) can be used to determine ϵ_n values from the photon-per-pulse measurements. Using data from the figures Fig. 1(c), Fig. S3(b), and Fig. S4(b) of Ref. [1], one can obtain that $\epsilon_3 \approx 4.6$, and $\epsilon_5 \approx 6$ for GaAs target, $\epsilon_3 \approx 4$ and $\epsilon_5 \approx 6$ for ZnO target, and $\epsilon_3 \approx 5.6$ and $\epsilon_5 \approx 5.8$ for Si target, respectively. The ratio C_3/C_5

can also be estimated from these figures. To proceed, we express the effective susceptibilities in a way that incorporates the transition between perturbative and low-intensity nonperturbative regimes. For this purpose, we write

$$\chi_n(|\alpha_0|) = \begin{cases} \chi_n^{(pert)} & \text{if } |\alpha_0| \leq \alpha_{(n)} \\ \chi_n^{(pert)} \left(\frac{\alpha_{(n)}}{|\alpha_0|} \right)^{n-\frac{\epsilon_n}{2}} & \text{if } |\alpha_0| > \alpha_{(n)} \end{cases}. \quad (56)$$

With the above considerations, susceptibilities are chosen so that they replicate the $\langle N_n(\tau) \rangle$ dependencies on the pulse energy reasonably well, while keeping in mind the limits of validity of the perturbative calculations.

In the following, we will assume that the driving pulse is of half-cycle duration, that is, $\tau = T/2$. Recall that while we have chosen the range of $|\alpha_0|$ to be of small values, it can be scaled up arbitrarily. The susceptibilities we have chosen for the three materials are listed in equations (57-62). Using these and the formulae of Sec. IV, we have calculated the physical quantities measured in Ref. [1]. The results of our analysis are shown on Fig. (6), Fig. (7) and Fig. (8), showing physical quantities as functions of $|\alpha_0|^2$, which read

$$\chi_3^{(\text{GaAs})}(|\alpha_0|) = \begin{cases} 0.069 & \text{if } |\alpha_0| \leq 1.05 \\ 0.069 \left(\frac{1.05}{|\alpha_0|} \right)^{0.7} & \text{if } |\alpha_0| > 1.05 \end{cases}, \quad (57)$$

$$\chi_5^{(\text{GaAs})}(|\alpha_0|) = \begin{cases} 0.01 & \text{if } |\alpha_0| \leq 0.735 \\ 0.01 \left(\frac{0.735}{|\alpha_0|} \right)^2 & \text{if } |\alpha_0| > 0.735 \end{cases}, \quad (58)$$

$$\chi_3^{(\text{Zno})}(|\alpha_0|) = \begin{cases} 0.041 & \text{if } |\alpha_0| \leq 1.3 \\ 0.041 \left(\frac{1.3}{|\alpha_0|} \right)^1 & \text{if } |\alpha_0| > 1.3 \end{cases}, \quad (59)$$

$$\chi_5^{(\text{Zno})}(|\alpha_0|) = \begin{cases} 0.035 & \text{if } |\alpha_0| \leq 0.377 \\ 0.035 \left(\frac{0.377}{|\alpha_0|} \right)^2 & \text{if } |\alpha_0| > 0.377 \end{cases}, \quad (60)$$

$$\chi_3^{(\text{Si})}(|\alpha_0|) = \begin{cases} 0.027 & \text{if } |\alpha_0| \leq 1.35 \\ 0.027 \left(\frac{1.35}{|\alpha_0|} \right)^{0.2} & \text{if } |\alpha_0| > 1.35 \end{cases}, \quad (61)$$

$$\chi_5^{(\text{Si})}(|\alpha_0|) = \begin{cases} 4.31 & \text{if } |\alpha_0| \leq 0.06 \\ 4.31 \left(\frac{0.06}{|\alpha_0|} \right)^{2.1} & \text{if } |\alpha_0| > 0.06 \end{cases}. \quad (62)$$

Comparing Fig. 6(a) to Fig. 1(b) of Ref. [1], one can see that the measured mean photons-per-pulse qualitatively corresponds to the calculated mean photon numbers $\langle N_3(\tau) \rangle$ and $\langle N_5(\tau) \rangle$, shown as red and blue curves on Fig. 6(a). The parameters have been chosen so that the ratio $\langle N_3(\tau) \rangle / \langle N_5(\tau) \rangle$ and the ratio of transition amplitudes $\alpha_{(3)}/\alpha_{(5)}$ correspond to the measured values. Fig. 6(b) shows the values of the auto-; and cross-correlation functions $\gamma_{33}(\tau)$, $\gamma_{55}(\tau)$ and $\gamma_{35}(\tau)$, respectively. The generally decreasing tendency with the pulse energy is reproduced up to the transition amplitude of the 3rd order harmonic $\alpha_{(3)}$. However, the values of these correlation functions are typically below 1, unlike the

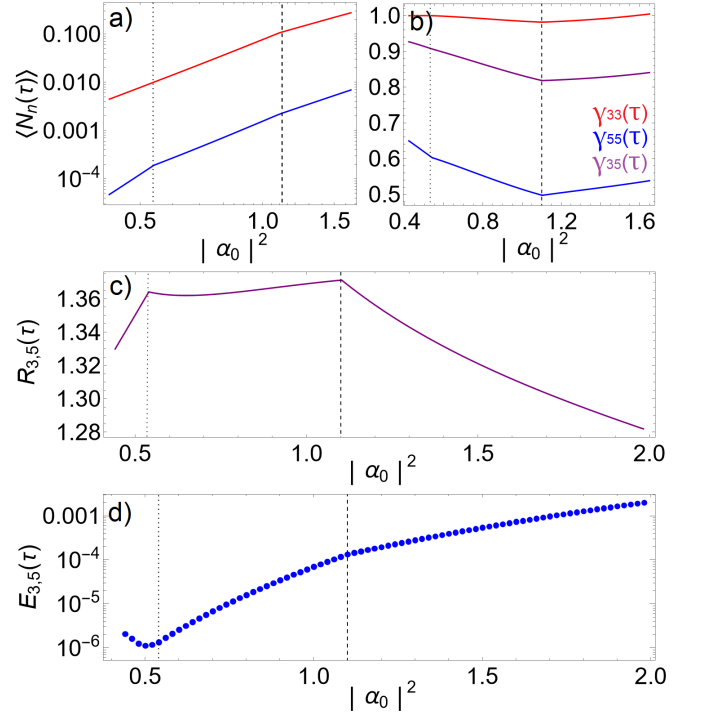


FIG. 6. Physical quantities as function of $|\alpha_0|^2$, using GaAs susceptibilities given by equations (57-58). Dashed and dotted lines show the transitions to the non-perturbative regime for the 3'rd and 5'th harmonics, respectively. a) Mean photon numbers $\langle N_3(\tau) \rangle$ (red) and $\langle N_5(\tau) \rangle$ (blue). b) Shows the photon auto-; and cross-correlation functions at the end of the interaction. Subfigure c) shows the $R_{3,5}(\tau)$ values. d) The logarithmic negativity $E_{3,5}(\tau)$.

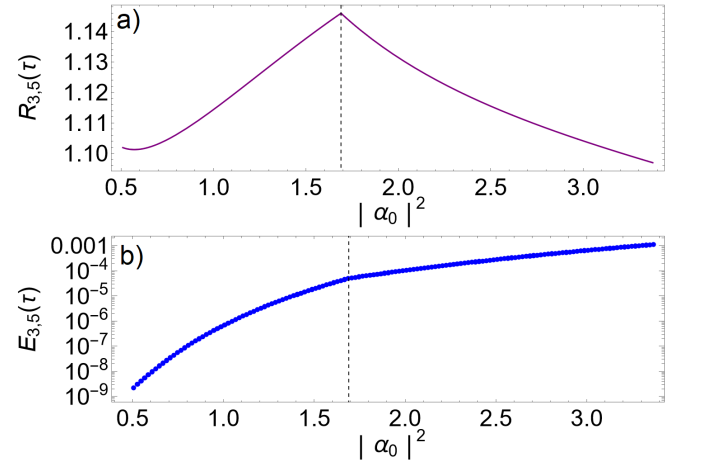


FIG. 7. Physical quantities as function of $|\alpha_0|^2$, using ZnO susceptibilities given by equations (59-60). a) $R_{3,5}(\tau)$ value and b) logarithmic negativity $E_{3,5}(\tau)$, respectively.

measured values. Nevertheless, valuable insight can be gained from the intensity-dependence of the correlation function: At transition amplitude $\alpha_{(n)}$, not only γ_{nn} , but the autocorrelation function of the other mode also expe-

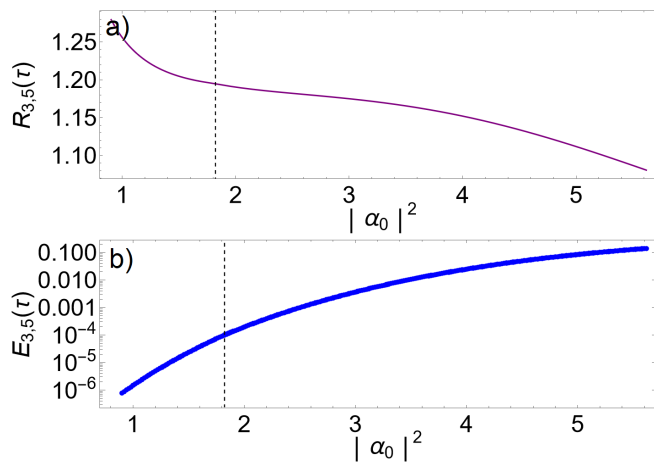


FIG. 8. Physical quantities as function of $|\alpha_0|^2$, using Si susceptibilities given by equations (61-62). The same quantities are listed as in Fig. 7.

riences a transition. This can also be observed to a lesser degree on plots of mean photon numbers $\langle N_n(\tau) \rangle$. The explanation is straightforward when observing Eq. (39) and Eq. (41). Since $\Omega_{n,0}$ contains all χ_n susceptibilities [see Eq. (36) and Eq. (35)], any transition in the largest susceptibilities will be imprinted in all photon numbers and related quantities. This observation may explain the simultaneous deviations of the measured photons-per-pulse of the 3rd and 5th harmonic, observable in Fig. S3(b) of Ref. [1].

We present the $R_{3,5}(\tau)$ values on Fig. 6(c), Fig. 7(a), and Fig. 8(a). The CBS-inequality violation, that is $R_{3,5}(\tau) > 1$, is reproduced as measured, implying the presence of nonclassical correlations in the pair of harmonic modes. One can see that the material-dependent α_n transition amplitudes can have a pronounced effect on the intensity-dependence of $R_{3,5}(\tau)$. While the calculated values are somewhat larger than the measured ones for the chosen parameters, the qualitative agreement is easy to check when comparing Fig. 6(c) to Fig. 3 of Ref. [1], and analogously Fig. 7(a) and Fig. 8(a) to Fig. S6 of Ref. [1]. Somewhat surprisingly, a plateau-like structure can be reproduced for the case of GaAs [Fig. 6(c)] between the transition pulse energies $|\alpha_{(5)}|^2$ and $|\alpha_{(3)}|^2$. For the case of ZnO, our model can imitate the moderately increasing tendency of $R_{3,5}(\tau)$ up to $|\alpha_{(3)}|^2$ pulse energy, followed by a slow decline [Fig. 7(c)]. For the Si target, our model predicts monotonously decreasing $R_{3,5}(\tau)$ values with increasing pulse energy, without particularly notable transition.

While nonclassical correlations have been both measured and can be reproduced by our calculation, it is not straightforward that the nonclassicality implies entanglement. We present the logarithmic negativities $E_{3,5}(\tau)$ as functions of pulse energy on Fig. 6(d), Fig. 7(b), and Fig. 8(b). The logarithmic negativity generally has an increasing tendency with the pulse energy, although for low pulse energies we observed decreasing tendencies as

well. Generally, the $R_{3,5}(\tau)$ values and the $E_{3,5}(\tau)$ functions have little correlation with increasing pulse energy. However, in cases of "well-structured" $R_{3,5}(\tau)$ functions [such as in Fig. 6(d)] the transition pulse energies are, to a small degree, imprinted on the negativity function. We note that the logarithmic negativities have not been measured directly, but our calculations support the interpretation that the arising nonclassicalities are, at least partially, in the form of entanglement.

Finally, we note that the problem of fitting parameters to perturbative results often becomes a trade-off between the validity of the results and the fidelity with which the data is reproduced. Furthermore, let us add that in some experiments, such as Ref. [32], the mean photon number of the driving pulse has been measured, instead of its intensity, leading to slightly different, although similar expressions.

VI. CONCLUSIONS

We have considered an effective quantum optical model of HHG, in which both the driving field and the harmonic radiation are quantized, while the material is included only through susceptibilities. Analogously to traditional models of harmonic generation, we have assumed that the dominant process is the simultaneous absorption of n photons from the driving field and emission of a photon into the n th harmonic mode. We have performed a perturbative calculation and analytically evaluated quantum optical quantities associated with single modes, and with pairs of modes. We have analyzed the behaviour of these quantities for various regimes of the HHG process.

We have found that nonclassicalities, comparable in magnitude to experimental measurements, emerge. These nonclassical properties include entanglement between harmonic modes and can be present in both perturbative and non-perturbative regimes. Furthermore, we have found that by fitting susceptibilities to the data of a recent experiment [1], our model could, for certain materials, reproduce characteristics of the intensity-dependence of the nonclassical correlation measure R .

As our model neglects the quantum state of the target material, the interpretation of the results is straightforward: By incorporating the depletion of the driving field during HHG, the back-action on the pump is naturally incorporated into our model. Consequently, the back-action modifies the quantum state of the driving field, leading to a modification in the quantum state of the harmonic modes. Ultimately, as a result of this, intermodal correlations and entanglement between the harmonics emerge.

Our approach has the advantage of not depending on specific properties of the target medium, except for the effective χ susceptibilities. Therefore, any feature of HHG that can be reproduced within our model can be considered a general aspect of HHG, not specific to the interaction material. We believe that theoretical research

in this field can benefit from our results, and provide further insight into the quantum aspects of HHG.

ACKNOWLEDGMENTS

We are thankful to Péter Földi and Sándor Varró for the useful suggestions with respect to the conceptual framework. This research was supported by the National Research, Development and Innovation Office, Hungary ("Quantum Information National Laboratory of Hungary" Grant No. 2022-2.1.1-NL-2022-00004, "Frontline" Research Excellence Programme Grant No. KKP133827, and Grant No. TKP2021-EGA-17).

Appendix A: Quantum optical quantities in perturbative approach

Below, we present the derivation of the quantum optical quantities used in Sec. IV, in a more general form. Here, we do not assume the initial condition used in the second half of section IV, and we let the lowest-order harmonic symbolically be n_1 instead of 2. The square norm is straightforward to express $\mathcal{N}(t) = 1 + \sum_{k=1}^N |\Theta_k|^2 t^4 + \sum_{k=0}^N \sum_{j=n_1}^N |\Omega_{j,k}|^2 t^6$. Below, we first give the mean photon numbers of the driving mode

$$\begin{aligned} \langle N_1(t) \rangle &= \frac{\langle \Psi | N_1 | \Psi \rangle}{\langle \Psi | \Psi \rangle} \\ &= \frac{1}{\mathcal{N}(t)} \langle \Psi' | N_1 + \alpha_0 e^{-i\omega t} a_1^\dagger + \alpha_0^* e^{i\omega t} a_1 + |\alpha_0|^2 | \Psi' \rangle \\ &= \frac{1}{\mathcal{N}(t)} \left[|\alpha_0|^2 \mathcal{N}(t) - (\Theta_1 \alpha_0^* + \Theta_1^* \alpha_0) t^2 \right. \\ &\quad \left. + \sum_{k=1}^N k |\Theta_k|^2 t^4 + \sum_{k=0}^N \sum_{j=n_1}^N k |\Omega_{j,k}|^2 t^6 \right. \\ &\quad \left. + \sum_{k=1}^N \sqrt{k+1} (\alpha_0 \Theta_{k+1}^* \Theta_k + \alpha_0^* \Theta_k^* \Theta_{k+1}) t^4 + \right. \\ &\quad \left. \sum_{k=0}^N \sum_{j=n_1}^N \sqrt{k+1} (\alpha_0 \Omega_{j,k+1}^* \Omega_{j,k} + \alpha_0^* \Omega_{j,k}^* \Omega_{j,k+1}) t^6 \right], \end{aligned} \quad (\text{A1})$$

and the mean photon number of the n 'th harmonic mode

$$\begin{aligned} \langle N_n(t) \rangle &= \frac{1}{\mathcal{N}(t)} \langle \Psi | N_n | \Psi \rangle \\ &= \frac{1}{\mathcal{N}(t)} \langle \Psi' | N_n - it\chi_n \alpha_0^n e^{-in\omega t} a_n^\dagger + it\chi_n \alpha_0^{*n} e^{in\omega t} a_n \\ &\quad + t^2 \chi_n^2 |\alpha_0|^{2n} | \Psi' \rangle = \frac{1}{\mathcal{N}(t)} \left[\chi_n^2 |\alpha_0|^{2n} t^2 \mathcal{N}(t) \right. \\ &\quad \left. + \sum_{k=0}^N |\Omega_{n,k}|^2 t^6 + \chi_n (\alpha_0^n \Omega_{n,0}^* + \alpha_0^{*n} \Omega_{n,0}) t^4 \right] \end{aligned}$$

$$- \chi_n \sum_{k=1}^N (\alpha_0^n \Theta_k \Omega_{n,k}^* + \alpha_0^{*n} \Theta_k^* \Omega_{n,k}) t^6 \Big], \quad (\text{A2})$$

respectively. The coherence functions are listed below. Autocoherence of the driving field mode is

$$\begin{aligned} G_{11}(t) &= \frac{1}{\mathcal{N}(t)} \langle \Psi' | (a_1^\dagger + \alpha_0^* e^{i\omega t}) (a_1^\dagger + \alpha_0^* e^{i\omega t}) \\ &\quad (a_1 + \alpha_0 e^{-i\omega t}) (a_1 + \alpha_0 e^{-i\omega t}) | \Psi' \rangle \\ &= \frac{1}{\mathcal{N}(t)} \langle \Psi' | a_1^{\dagger 2} a_1^2 + 2(\alpha e^{-i\omega t} a_1^{\dagger 2} a_1 + \alpha^* e^{i\omega t} a_1^\dagger a_1^2) \\ &\quad + \alpha_0^2 e^{-i2\omega t} a_1^{\dagger 2} + \alpha_0^2 e^{i2\omega t} a_1^2 + 4|\alpha_0|^2 a_1^\dagger a_1 \\ &\quad + 2|\alpha_0|^2 (\alpha_0 e^{-i\omega t} a_1^\dagger + \alpha_0^* e^{i\omega t} a_1) + |\alpha_0|^4 | \Psi' \rangle \\ &= \frac{1}{\mathcal{N}(t)} \left[|\alpha_0|^4 \mathcal{N}(t) + \sum_{k=1}^N |\Theta_k|^2 [k(k-1) + 4|\alpha|^2 k] t^4 \right. \\ &\quad \left. + \sum_{k=0}^N \sum_{j=n_1}^N |\Omega_{j,k}|^2 [k(k-1) + 4|\alpha_0|^2 k] t^6 \right. \\ &\quad \left. - 2|\alpha_0|^2 (\Theta_1 \alpha_0^* + \Theta_1^* \alpha_0) t^2 \right. \\ &\quad \left. + 2|\alpha_0|^2 \sum_{k=1}^N \sqrt{k+1} (\alpha_0 \Theta_{k+1}^* \Theta_k + \alpha_0^* \Theta_k^* \Theta_{k+1}) t^4 \right. \\ &\quad \left. + 2|\alpha_0|^2 \sum_{k=0}^N \sum_{j=n_1}^N \sqrt{k+1} (\alpha_0 \Omega_{j,k+1}^* \Omega_{j,k} + \alpha_0^* \Omega_{j,k}^* \Omega_{j,k+1}) t^6 \right. \\ &\quad \left. - \sqrt{2} (\alpha_0^{*2} \Theta_2 + \alpha_0^2 \Theta_2^*) t^2 \right. \\ &\quad \left. + \sum_{k=1}^N \sqrt{k+1} \sqrt{k+2} (\alpha_0^{*2} \Theta_k^* \Theta_{k+2} + \alpha_0^2 \Theta_{k+2}^* \Theta_k) t^4 \right. \\ &\quad \left. + \sum_{k=0}^N \sum_{j=n_1}^N \sqrt{k+1} \sqrt{k+2} (\alpha_0^{*2} \Omega_{j,k}^* \Omega_{j,k+2} + \alpha_0^2 \Omega_{j,k+2}^* \Omega_{j,k}) t^6 \right. \\ &\quad \left. + 2 \sum_{k=0}^N k \sqrt{k+1} (\alpha_0 \Theta_{k+1}^* \Theta_k + \alpha_0^* \Theta_k^* \Theta_{k+1}) t^4 \right], \end{aligned} \quad (\text{A3})$$

and for the n 'th harmonic mode, $n \neq 1$, it is

$$\begin{aligned} G_{nn}(t) &= \frac{1}{\mathcal{N}(t)} \langle \Psi' | (a_n^\dagger + it\chi_n \alpha_0^{*n} e^{in\omega t}) (a_n^\dagger + it\chi_n \alpha_0^{*n} e^{in\omega t}) \\ &\quad \times (a_n - it\chi_n \alpha_0^n e^{-in\omega t}) (a_n - it\chi_n \alpha_0^n e^{-in\omega t}) | \Psi' \rangle = \frac{1}{\mathcal{N}(t)} \\ &\quad \times \langle \Psi' | a_n^{\dagger 2} a_n^2 - 2(it\chi_n \alpha_0^n e^{-in\omega t} a_n^{\dagger 2} a_n - it\chi_n \alpha_0^{*n} e^{in\omega t} a_n^\dagger a_n^2) \\ &\quad - \chi_n^2 t^2 (\alpha_0^{2n} e^{-i2n\omega t} a_n^{\dagger 2} + \alpha_0^{*2n} e^{i2n\omega t} a_n^2) + 4\chi_n^2 t^2 |\alpha_0|^{2n} a_n^\dagger a_n \\ &\quad - 2i\chi_n^3 |\alpha_0|^{2n} t^3 (\alpha_0^n e^{-in\omega t} a_n^\dagger - \alpha_0^{*n} e^{in\omega t} a_n) + \chi_n^4 t^4 |\alpha_0|^{4n} | \Psi' \rangle \\ &= \frac{1}{\mathcal{N}(t)} \left[4\chi_n^2 |\alpha_0|^{2n} \sum_{k=0}^N |\Omega_{n,k}|^2 t^8 \right. \\ &\quad \left. + 2\chi_n^3 |\alpha_0|^{2n} (\alpha^{*n} \Omega_{n,0} + \alpha^n \Omega_{n,0}^*) t^6 + \chi_n^4 t^4 |\alpha_0|^{4n} \mathcal{N}(t) \right] \end{aligned}$$

$$-2\chi_n^3|\alpha_0|^{2n}\sum_{k=1}^N(\alpha_0^{*n}\Omega_{n,k}\Theta_k^*+\alpha_0^n\Omega_{n,k}^*\Theta_k)t^8]. \quad (\text{A4})$$

Intermodal cross-coherence functions between the excitation mode and the n 'th harmonic mode is

$$\begin{aligned} G_{1n}(t) &= \frac{1}{\mathcal{N}(t)}\langle\Psi'| (N_1 + \alpha_0 e^{-i\omega t} a_1^\dagger + \alpha_0^* e^{i\omega t} a_1 + |\alpha_0|^2) \\ & (N_n - it\chi_n \alpha_0^n e^{-in\omega t} a_n^\dagger + it\chi_n \alpha_0^{*n} e^{in\omega t} a_n + t^2 \chi_n^2 |\alpha_0|^{2n}) |\Psi'\rangle \\ &= \frac{1}{\mathcal{N}(t)}\langle\Psi'| N_1 N_n + N_n (\alpha_0 e^{-i\omega t} a_1^\dagger + \alpha_0^* e^{i\omega t} a_1 + |\alpha_0|^2) \\ & + i\chi_n t (\alpha_0^{*n} e^{in\omega t} N_1 a_n - \alpha_0^n e^{-in\omega t} N_1 a_n^\dagger) + \chi_n^2 |\alpha_0|^{2n} t^2 N_1 \\ & + i\chi_n t (\alpha_0^{*(n+1)} e^{i(n+1)\omega t} a_1 a_n - \alpha_0^{(n+1)} e^{-i(n+1)\omega t} a_1^\dagger a_n^\dagger) \\ & + \alpha_0^{*n} \alpha_0 e^{i(n-1)\omega t} a_1^\dagger a_n - \alpha_0^n \alpha_0^* e^{-i(n-1)\omega t} a_1 a_n^\dagger \\ & + i\chi_n t |\alpha_0|^2 (\alpha_0^{*n} e^{in\omega t} a_n - \alpha_0^n e^{-in\omega t} a_n^\dagger) \\ & + \chi_n^2 |\alpha_0|^{2n} (\alpha_0 e^{-i\omega t} a_1^\dagger + \alpha_0^* e^{i\omega t} a_1 + |\alpha_0|^2) t^2 |\Psi'\rangle \\ &= \frac{1}{\mathcal{N}(t)} \left[\sum_{k=0}^N |\Omega_{n,k}|^2 t^6 (k + |\alpha_0|^2) \right. \\ & + \sum_{k=0}^N (\alpha_0 \Omega_{n,k+1}^* \Omega_{n,k} + \alpha_0^* \Omega_{n,k}^* \Omega_{n,k+1}) \sqrt{k+1} t^6 \\ & + \chi_n^2 |\alpha_0|^{2n} t^6 \left(\sum_{k=1}^N k |\Theta_k|^2 + \sum_{k=0}^N \sum_{j=n_1}^N k |\Omega_{j,k}|^2 t^2 \right) \\ & - \chi_n t^6 \sum_{k=1}^N k (\alpha_0^{*n} \Theta_k^* \Omega_{n,k} + \alpha_0^n \Theta_k \Omega_{n,k}^*) \\ & + \chi_n t^4 \left(\alpha_0^{*(n+1)} \Omega_{n,1} + \alpha_0^{(n+1)} \Omega_{n,1}^* \right) \\ & - \sum_{k=2}^N \sqrt{k} (\alpha_0^{*(n+1)} \Theta_{k-1}^* \Omega_{n,k} + \alpha_0^{(n+1)} \Theta_{k-1} \Omega_{n,k}^*) t^2 \\ & \left. - \chi_n |\alpha_0|^{2n} t^6 \right) \\ & \times \left(\sum_{k=0}^N \sqrt{k+1} (\alpha_0^{*(n-1)} \Theta_{k+1}^* \Omega_{n,k} + \alpha_0^{(n-1)} \Theta_{k+1} \Omega_{n,k}^*) \right) \\ & + \chi_n^2 |\alpha_0|^{2n+2} t^2 \mathcal{N}(t) + \chi_n |\alpha_0|^{2n} t^4 \\ & \times \left(\alpha_0^{*n} \Omega_{n,0} + \alpha_0^n \Omega_{n,0}^* - \sum_{k=1}^N (\alpha_0^{*n} \Theta_k^* \Omega_{n,k} + \alpha_0^n \Theta_k \Omega_{n,k}^*) t^2 \right) \\ & - \chi_n^2 |\alpha_0|^{2n} t^4 (\alpha_0^* \Theta_1 + \alpha_0 \Theta_1^*) \\ & + \chi_n^2 |\alpha_0|^{2n} t^2 \left(\sum_{k=1}^N \sqrt{k+1} (\alpha_0^* \Theta_k^* \Theta_{k+1} + \alpha_0 \Theta_k \Theta_{k+1}^*) t^4 \right) \end{aligned}$$

$$+ \sum_{k=0}^N \sum_{j=n_1}^N \sqrt{k+1} (\alpha_0^* \Omega_{j,k}^* \Omega_{j,k+1} + \alpha_0 \Omega_{j,k} \Omega_{j,k+1}^*) t^6 \Big], \quad (\text{A5})$$

and between the n 'th and m 'th harmonic modes, $n \neq m \neq 1$, it is

$$\begin{aligned} G_{nm}(t) &= \frac{1}{\mathcal{N}(t)}\langle\Psi'| (N_n \\ & - it\chi_n (\alpha_0^n e^{-in\omega t} a_n^\dagger - \alpha_0^{*n} e^{in\omega t} a_n) + t^2 \chi_n^2 |\alpha_0|^{2n}) \\ & (N_m - it\chi_m (\alpha_0^m e^{-im\omega t} a_m^\dagger - \alpha_0^{*m} e^{im\omega t} a_m) \\ & + t^2 \chi_m^2 |\alpha_0|^{2m}) |\Psi'\rangle = \frac{1}{\mathcal{N}(t)} \langle\Psi| N_n N_m \\ & - i\chi_n t (\alpha_0^n e^{-in\omega t} a_n^\dagger N_m - \alpha_0^{*n} e^{in\omega t} a_n N_m) \\ & + i\chi_m t (\alpha_0^{*m} e^{im\omega t} a_m N_n - \alpha_0^m e^{-im\omega t} a_m^\dagger N_n) \\ & + N_n \chi_m^2 t^2 |\alpha_0|^{2m} + N_m \chi_n^2 t^2 |\alpha_0|^{2n} \\ & - \chi_n \chi_m t^2 (\alpha_0^{n+m} e^{-i(n+m)\omega t} a_n^\dagger a_m^\dagger \\ & + \alpha_0^{*(n+m)} e^{i(n+m)\omega t} a_n a_m) \\ & + \chi_n \chi_m t^2 (\alpha_0^n \alpha_0^{*m} e^{-i(n-m)\omega t} a_n^\dagger a_m \\ & + \alpha_0^{*n} \alpha_0^m e^{i(n-m)\omega t} a_n a_m^\dagger) \\ & + \chi_n^2 \chi_m^2 t^4 |\alpha_0|^{2n+2m} - i\chi_n \chi_m^2 |\alpha_0|^{2m} t^3 \\ & (e^{-in\omega t} \alpha_0^n a_n^\dagger - e^{in\omega t} \alpha_0^{*n} a_n) \\ & - i\chi_m \chi_n^2 |\alpha_0|^{2n} t^3 (e^{-im\omega t} \alpha_0^m a_m^\dagger - e^{im\omega t} \alpha_0^{*m} a_m) |\Psi\rangle \\ &= \frac{1}{\mathcal{N}(t)} \left[\sum_{k=0}^N [|\Omega_{n,k}|^2 \chi_m^2 |\alpha_0|^{2m} + |\Omega_{m,k}|^2 \chi_n^2 |\alpha_0|^{2n}] t^8 \right. \\ & \left. + \chi_n^2 \chi_m^2 t^4 |\alpha_0|^{2n+2m} \mathcal{N}(t) \right. \\ & + \chi_n \chi_m t^8 \sum_{k=0}^N (\alpha_0^n \alpha_0^{*m} \Omega_{m,k} \Omega_{n,k}^* + \alpha_0^m \alpha_0^{*n} \Omega_{n,k} \Omega_{m,k}^*) \\ & + \chi_n \chi_m^2 t^6 |\alpha_0|^{2m} (\alpha_0^n \Omega_{n,0}^* + \alpha_0^{*n} \Omega_{n,0}) \\ & + \chi_n^2 \chi_m t^6 |\alpha_0|^{2n} (\alpha_0^m \Omega_{m,0}^* + \alpha_0^{*m} \Omega_{m,0}) \\ & - \chi_n \chi_m^2 t^8 |\alpha_0|^{2m} \sum_{k=1}^N (\alpha_0^n \Omega_{n,k}^* \Theta_k + \alpha_0^{*n} \Omega_{n,k} \Theta_k^*) \\ & \left. - \chi_m \chi_n^2 t^8 |\alpha_0|^{2n} \sum_{k=1}^N (\alpha_0^m \Omega_{m,k}^* \Theta_k + \alpha_0^{*m} \Omega_{m,k} \Theta_k^*) \right]. \quad (\text{A6}) \end{aligned}$$

Appendix B: Density matrix of the field

Here, we present the density matrix of the total electromagnetic field $\rho^{(2)}(t)$, based on the perturbatively calculated quantum state defined by Eq. (31), as well as that of various sub-systems that we investigated in our work. Note

that here, we let the lowest-order of harmonics be set symbolically to n_1 instead of 2. By substituting Eq. (31) into $\rho^{(2)}(t) = |\Psi'(t)\rangle\langle\Psi'(t)|^{(2)}$ and expanding, we get

$$\begin{aligned}
\rho^{(2)}(t) = & \left[|0\rangle\otimes_n|0\rangle_n - \sum_{k=1}^N \Theta_k t^2 |k\rangle\otimes_n|0\rangle_n e^{-ik\omega t} - i \sum_{k=0}^N \sum_{j=n_1}^N \Omega_{j,k} t^3 |k\rangle|1\rangle_j \otimes_{n\neq j} |0\rangle_n e^{-i(k+j)\omega t} \right] \\
& \left[\langle 0|\otimes_n\langle 0|_n - \sum_{k=1}^N \Theta_k^* t^2 \langle k|\otimes_n\langle 0|_n e^{ik\omega t} + i \sum_{k=0}^N \sum_{j=n_1}^N \Omega_{j,k}^* t^3 \langle k|\langle 1|_j \otimes_{n\neq j} \langle 0|_n e^{i(k+j)\omega t} \right] \\
& = |0\rangle\langle 0|\otimes_n|0\rangle_n\langle 0|_n + \sum_{k,k'=1}^N \Theta_k \Theta_{k'}^* t^4 e^{i(k'-k)\omega t} |k\rangle\langle k'|\otimes_n|0\rangle_n\langle 0|_n \\
& - \sum_{k=1}^N \Theta_k^* t^2 e^{ik\omega t} |0\rangle\langle k|\otimes_n|0\rangle_n\langle 0|_n - \sum_{k=1}^N \Theta_k t^2 e^{-ik\omega t} |k\rangle\langle 0|\otimes_n|0\rangle_n\langle 0|_n \\
& + i \sum_{k=0}^N \sum_{j=n_1}^N \Omega_{j,k}^* t^3 e^{i(k+j)\omega t} |0\rangle\langle k|\otimes_j\langle 1|_j \otimes_{n\neq j} |0\rangle_n\langle 0|_n - i \sum_{k=0}^N \sum_{j=n_1}^N \Omega_{j,k} t^3 e^{-i(k+j)\omega t} |k\rangle\langle 0|\otimes_j\langle 0|_j \otimes_{n\neq j} |0\rangle_n\langle 0|_n \\
& + \sum_{k,k'=0}^N \sum_{j,j'=n_1}^N \Omega_{j,k} \Omega_{j',k'}^* t^6 e^{i(k'-k+j'-j)\omega t} |k\rangle\langle k'|\otimes_j\langle 1|_j \otimes_{n\neq j,m\neq j'} |0\rangle_n\langle 0|_m \\
& - i \sum_{\substack{k=1 \\ k'=0}}^N \sum_{j=n_1}^N \Theta_k \Omega_{j,k'}^* t^5 e^{i(k'-k+j)\omega t} |k\rangle\langle k'|\otimes_j\langle 1|_j \otimes_{n\neq j} |0\rangle_n\langle 0|_n + i \sum_{\substack{k=1 \\ k'=0}}^N \sum_{j=n_1}^N \Theta_k^* \Omega_{j,k'} t^5 e^{-i(k'-k+j)\omega t} |k'\rangle\langle k|\otimes_j\langle 0|_j \otimes_{n\neq j} |0\rangle_n\langle 0|_n .
\end{aligned}$$

Tracing out the excitation mode leads us to the density matrix associated with the collective harmonic field. Although not written explicitly, the index n runs from n_1 to N :

$$\begin{aligned}
\rho'_{\text{harm}}(t) \equiv \sum_i \langle i|\rho^{(2)}(t)|i\rangle = & \left[1 + \sum_{k=1}^N |\Theta_k|^2 t^4 \right] \otimes_n |0\rangle_n\langle 0|_n + \\
& it^3 \sum_{j=n_1}^N \left[\Omega_{j,0}^* e^{ij\omega t} |0\rangle_j\langle 1|_j - \Omega_{j,0} e^{-ij\omega t} |1\rangle_j\langle 0|_j \right] \otimes_{n\neq j} |0\rangle_n\langle 0|_n \\
& - i \sum_{k=1}^N \sum_{j=n_1}^N \Theta_k \Omega_{j,k}^* t^5 e^{ij\omega t} |0\rangle_j\langle 1|_j \otimes_{n\neq j} |0\rangle_n\langle 0|_n \\
& + i \sum_{k=1}^N \sum_{j=n_1}^N \Theta_k^* \Omega_{j,k} t^5 e^{-ij\omega t} |1\rangle_j\langle 0|_j \otimes_{n\neq j} |0\rangle_n\langle 0|_n + \\
& \sum_{k=0}^N \sum_{j,j'=n_1}^N \Omega_{j,k} \Omega_{j',k}^* t^6 e^{i(j'-j)\omega t} |1\rangle_j\langle 1|_{j'} \otimes_{n\neq j,m\neq j'} |0\rangle_n\langle 0|_m .
\end{aligned} \tag{B1}$$

Tracing out all but the n 'th harmonic mode results in the density matrix associated with the subsystem of a single harmonic mode

$$\rho'_{\text{n}^{\text{th}}}(t) = \sum_{k=0}^N |\Omega_{n,k}|^2 t^6 |1\rangle_n\langle 1|_n$$

$$\begin{aligned}
& + \left[1 + \sum_{k=1}^N |\Theta_k|^2 t^4 + \sum_{k=0}^N \sum_{\substack{j=n_1 \\ j\neq n}}^N |\Omega_{j,k}|^2 t^6 \right] |0\rangle_n\langle 0|_n \\
& + it^3 \left[\Omega_{n,0}^* e^{in\omega t} |0\rangle_n\langle 1|_n - \Omega_{n,0} e^{-in\omega t} |1\rangle_n\langle 0|_n \right] \\
& - it^5 \sum_{k=1}^N \left[\Theta_k \Omega_{n,k}^* e^{in\omega t} |0\rangle_n\langle 1|_n - \Theta_k^* \Omega_{n,k} e^{-in\omega t} |1\rangle_n\langle 0|_n \right] .
\end{aligned} \tag{B2}$$

To evaluate the entanglement between two harmonic modes, starting from $\rho'_{\text{harm}}(t)$, one needs to trace out all but the n 'th and m 'th harmonic modes. This leads to

$$\begin{aligned}
\rho'_{\text{nm}}(t) = & \left[1 + \sum_{k=1}^N |\Theta_k|^2 t^4 \right] |0\rangle_n\langle 0|_n |0\rangle_m\langle 0|_m \\
& + it^3 \left[\Omega_{n,0}^* e^{in\omega t} |0\rangle_n\langle 1|_n - \Omega_{n,0} e^{-in\omega t} |1\rangle_n\langle 0|_n \right] |0\rangle_m\langle 0|_m \\
& + it^3 \left[\Omega_{m,0}^* e^{im\omega t} |0\rangle_m\langle 1|_m - \Omega_{m,0} e^{-im\omega t} |1\rangle_m\langle 0|_m \right] |0\rangle_n\langle 0|_n \\
& - i \sum_{k=1}^N \Theta_k \Omega_{n,k}^* t^5 e^{in\omega t} |0\rangle_n\langle 1|_n |0\rangle_m\langle 0|_m \\
& - i \sum_{k=1}^N \Theta_k \Omega_{m,k}^* t^5 e^{im\omega t} |0\rangle_m\langle 1|_m |0\rangle_n\langle 0|_n
\end{aligned}$$

$$\begin{aligned}
& +i \sum_{k=1}^N \Theta_k^* \Omega_{n,k} t^5 e^{-in\omega t} |1\rangle_n \langle 0|_n |0\rangle_m \langle 0|_m \\
& +i \sum_{k=1}^N \Theta_k^* \Omega_{m,k} t^5 e^{-im\omega t} |1\rangle_m \langle 0|_m |0\rangle_n \langle 0|_n \\
& + \sum_{k=0}^N \Omega_{n,k} \Omega_{m,k}^* t^6 e^{i(m-n)\omega t} |1\rangle_n \langle 1|_m |0\rangle_m \langle 0|_n \\
& + \sum_{k=0}^N \Omega_{m,k} \Omega_{n,k}^* t^6 e^{i(n-m)\omega t} |1\rangle_m \langle 1|_n |0\rangle_n \langle 0|_m \\
& + \sum_{k=0}^N \Omega_{n,k} \Omega_{n,k}^* t^6 |1\rangle_n \langle 1|_n |0\rangle_m \langle 0|_m \\
& + \sum_{k=0}^N \Omega_{m,k} \Omega_{m,k}^* t^6 |1\rangle_m \langle 1|_m |0\rangle_n \langle 0|_n \\
& + \sum_{k=0}^N \sum_{j=n_1, j \neq n, m} \Omega_{j,k} \Omega_{j,k}^* t^6 |0\rangle_n \langle 0|_n |0\rangle_m \langle 0|_m, \quad (\text{B3})
\end{aligned}$$

which, after simplification and by introducing the $|ij\rangle\langle kl| \equiv |i\rangle_n |j\rangle_m \langle k|_n \langle l|_m$ notation, can be rewritten as:

$$\begin{aligned}
\rho_{\text{nm}}^{(2)}(t) = & \left[1 + \sum_{k=1}^N |\Theta_k|^2 t^4 + \sum_{k=0}^N \sum_{\substack{j=n_1 \\ j \neq n, m}} |\Omega_{j,k}|^2 t^6 \right] |00\rangle\langle 00| \\
& + it^3 \left[\Omega_{n,0}^* e^{in\omega t} |00\rangle\langle 10| - \Omega_{n,0} e^{-in\omega t} |10\rangle\langle 00| \right] \\
& + it^3 \left[\Omega_{m,0}^* e^{im\omega t} |00\rangle\langle 01| - \Omega_{m,0} e^{-im\omega t} |01\rangle\langle 00| \right] \\
& - it^5 \sum_{k=1}^N \left[\Theta_k \Omega_{n,k}^* e^{in\omega t} |00\rangle\langle 10| + \Theta_k \Omega_{m,k}^* e^{im\omega t} |00\rangle\langle 01| \right] \\
& + it^5 \sum_{k=1}^N \left[\Theta_k^* \Omega_{n,k} e^{-in\omega t} |10\rangle\langle 00| + \Theta_k^* \Omega_{m,k} e^{-im\omega t} |01\rangle\langle 00| \right] \\
& + \sum_{k=0}^N \Omega_{n,k} \Omega_{m,k}^* t^6 e^{i(m-n)\omega t} |10\rangle\langle 01| \\
& + \sum_{k=0}^N \Omega_{m,k} \Omega_{n,k}^* t^6 e^{i(n-m)\omega t} |01\rangle\langle 10|
\end{aligned}$$

$$+ \sum_{k=0}^N |\Omega_{n,k}|^2 t^6 |10\rangle\langle 10| + \sum_{k=0}^N |\Omega_{m,k}|^2 t^6 |01\rangle\langle 01|. \quad (\text{B4})$$

This, together with its partial transpose with respect to the mode indexed with n , can be represented in matrix form as:

$$\rho_{\text{nm}}^{(2)}(t) = \begin{bmatrix} a & b & c & 0 \\ b^* & d & e & 0 \\ c^* & e^* & f & 0 \\ 0 & 0 & 0 & 0 \end{bmatrix}, \quad \left(\rho_{\text{nm}}^{(2)}(t) \right)^{\Gamma_n} = \begin{bmatrix} a & b & c^* & e^* \\ b^* & d & 0 & 0 \\ c & 0 & f & 0 \\ e & 0 & 0 & 0 \end{bmatrix}, \quad (\text{B5})$$

where

$$\begin{aligned}
a & \equiv 1 + \sum_{k=1}^N |\Theta_k|^2 t^4 + \sum_{k=0}^N \sum_{\substack{j=n_1 \\ j \neq n, m}} |\Omega_{j,k}|^2 t^6, \\
b & \equiv it^3 \Omega_{m,0}^* e^{im\omega t} - it^5 \sum_{k=1}^N \Theta_k \Omega_{m,k}^* e^{im\omega t}, \\
c & \equiv it^3 \Omega_{n,0}^* e^{in\omega t} - it^5 \sum_{k=1}^N \Theta_k \Omega_{n,k}^* e^{in\omega t}, \\
d & \equiv \sum_{k=0}^N |\Omega_{m,k}|^2 t^6, \quad f \equiv \sum_{k=0}^N |\Omega_{n,k}|^2 t^6, \\
e & \equiv \sum_{k=0}^N \Omega_{m,k} \Omega_{n,k}^* t^6 e^{i(n-m)\omega t}.
\end{aligned}$$

For the sake of completeness, let us remind the reader that when determining the Wigner-function from a density-operator, the decomposition $\rho = \sum_{m,n} \rho_{m,n} |m\rangle\langle n|$ can be used, with which the Wigner-function can be written as

$$W(q, p) = \sum_{m,n} \rho_{m,n} W_{mn}(q, p). \quad (\text{B6})$$

Here

$$W_{mn}(q, p) = \frac{(-1)^m}{\pi} \langle n | \mathcal{D}(2\alpha) | m \rangle, \quad (\text{B7})$$

and

$$\langle n | \mathcal{D}(2\alpha) | m \rangle = \begin{cases} \sqrt{\frac{n!}{m!}} e^{-2|\alpha|^2} (-\alpha^*)^{m-n} L_n^{m-n}(4|\alpha|^2) & m \geq n \\ \sqrt{\frac{m!}{n!}} e^{-2|\alpha|^2} (\alpha)^{n-m} L_m^{n-m}(4|\alpha|^2) & m < n \end{cases}. \quad (\text{B8})$$

- [1] D. Theidel et al., PRX Quantum **5**, 040319 (2024), URL <https://link.aps.org/doi/10.1103/PRXQuantum.5.040319>.
[2] W. Asavanant and A. Furusawa, Phys. Rev. A **109**, 040101 (2024).

- [3] S. M. Barnett et al., Prog. Quantum Electron. **54**, 19 (2017), ISSN 0079-6727, URL <https://www.sciencedirect.com/science/article/pii/S0079672717300277>.
[4] X. Shi, W. W. Lee, A. Karnieli, L. M. Lohse, A. Gorkach,

- L. W. W. Wong, T. Salditt, S. Fan, I. Kaminer, and L. J. Wong, *Prog. Quantum Electron.* **102**, 100577 (2025), ISSN 0079-6727, URL <https://www.sciencedirect.com/science/article/pii/S0079672725000254>.
- [5] P. D. Drummond and M. Hillery, *The Quantum Theory of Nonlinear Optics* (Cambridge University Press, Cambridge, 2014).
- [6] M. Ferray, A. L’Huillier, X. Li, L. Lompre, G. Mainfray, and C. Manus, *J. Phys. B* **21**, L31 (1988).
- [7] R. M. Potvliege and R. Shakeshaft, *Phys. Rev. A* **40**, 3061 (1989), URL <https://link.aps.org/doi/10.1103/PhysRevA.40.3061>.
- [8] S. Ghimire, A. D. DiChiara, E. Sistrunk, P. Agostini, L. F. DiMauro, and D. A. Reis, *Nat. Physics* **7**, 138 (2011).
- [9] M. Lewenstein, P. Balcou, M. Y. Ivanov, A. L’Huillier, and P. B. Corkum, *Phys. Rev. A* **49**, 2117 (1994), URL <https://link.aps.org/doi/10.1103/PhysRevA.49.2117>.
- [10] J. Bergou and S. Varró, *J. Phys. A* **14**, 2281 (1981).
- [11] M. Kuchiev and V. Ostrovsky, *J. Phys. B* **32**, L189 (1999).
- [12] J. Gao, F. Shen, and J. Eden, *Phys. Rev. A* **61**, 043812 (2000).
- [13] L. Gao, X. Li, P. Fu, and R. Guo, *Phys. Rev. A* **61**, 063407 (2000).
- [14] J. B. Bertrand, H. J. Wörner, H.-C. Bandulet, E. Bisson, M. Spanner, J.-C. Kieffer, D. M. Villeneuve, and P. B. Corkum, *Phys. Rev. Lett.* **106**, 023001 (2011), URL <https://link.aps.org/doi/10.1103/PhysRevLett.106.023001>.
- [15] C. Yu, J. Zhang, Z.-W. Sun, Z. Sun, and D.-S. Guo, *Front. Phys.* **10**, 1 (2015).
- [16] I. K. Kominis, G. Kolliopoulos, D. Charalambidis, and P. Tzallas, *Phys. Rev. A* **89**, 063827 (2014).
- [17] L. Argenti, S. Chattopadhyay, M. Chini, N. Douguet, and C. Marante, in *ATTO 8th International Conference on Attosecond Science and Technology (Book of Abstracts)* (2022), URL https://sciences.ucf.edu/physics/atto/wp-content/uploads/sites/28/2022/06/ATTOVIII_BOA_June21.pdf.
- [18] A. Gombkötő, S. Varró, Z. Keresztes, B. Gábor, and P. Földi, in *Kvantumelektronika 2021: IX. Szimpózium a hazai kvantumelektronikai kutatások eredményeiről* (University of Szeged, Szeged, 2021), pp. 64–68, URL <https://api.semanticscholar.org/CorpusID:234339486>.
- [19] L. Argenti, M. Chini, and L. Fang, *Proceedings of the 8th International Conference on Attosecond Science and Technology* (Springer, 2024), ISBN 0930-8989.
- [20] P. Stammer and M. Lewenstein, *Acta Phys. Pol. A* **143**, S42 (2023), URL https://appol.ifpan.edu.pl/index.php/appa/article/view/143_s42.
- [21] J. Rivera-Dean, P. Stammer, A. S. Maxwell, T. Lamprou, A. F. Ordóñez, E. Pisanty, P. Tzallas, M. Lewenstein, and M. F. Ciappina, *Quantum Optical Analysis of High-Order Harmonic Generation in Semiconductors* (????), chap. 7, pp. 139–183.
- [22] N. Rivera, *Nanophotonics* **14**, 1837 (2025), URL <https://doi.org/10.1515/nanoph-2024-0605>.
- [23] P. Földi, I. Magashgyi, A. Gombkötő, and S. Varró, *Photonics* **8**, 263 (2021), ISSN 2304-6732.
- [24] S. Varró, *Photonics* **8**, 269 (2021), ISSN 2304-6732.
- [25] U. Bhattacharya, T. Lamprou, A. S. Maxwell, A. Ordóñez, E. Pisanty, J. Rivera-Dean, P. Stammer, M. F. Ciappina, M. Lewenstein, and P. Tzallas, *Rep. Prog. Phys.* **86**, 094401 (2023), URL <https://doi.org/10.1088/1361-6633/acea31>.
- [26] Y. S. Aklilu and K. Varga, *Phys. Rev. A* **110**, 043119 (2024), URL <https://link.aps.org/doi/10.1103/PhysRevA.110.043119>.
- [27] C. S. Lange and L. B. Madsen, *Phys. Rev. A* **111**, 013113 (2025), URL <https://link.aps.org/doi/10.1103/PhysRevA.111.013113>.
- [28] J.-H. Mun, S.-H. Jang, and S. K. Nam, *Phys. Rev. A* **110**, 043115 (2024), URL <https://link.aps.org/doi/10.1103/PhysRevA.110.043115>.
- [29] J. Rivera-Dean, T. Lamprou, E. Pisanty, M. F. Ciappina, P. Tzallas, M. Lewenstein, and P. Stammer, *Phys. Rev. A* **112**, 013110 (2025), URL <https://link.aps.org/doi/10.1103/PhysRevA.112.013110>.
- [30] T. Lamprou, P. Stammer, J. Rivera-Dean, N. Tsatrafyllis, M. F. Ciappina, M. Lewenstein, and P. Tzallas, *J. Phys. B: At. Mol. Opt. Phys.* **58**, 132001 (2025), URL <https://doi.org/10.1088/1361-6455/add9fe>.
- [31] N. Tsatrafyllis et al., *Phys. Rev. Lett.* **122**, 193602 (2019).
- [32] A. Rasputnyi, Z. Chen, M. Birk, O. Cohen, I. Kaminer, M. Krüger, D. Seletskiy, M. Chekhova, and F. Tani, *Nat. Phys.* **20**, 1960 (2024), URL <https://doi.org/10.1038/s41567-024-02659-x>.
- [33] A. Nayak et al., *Nat. Commun.* **16**, 1428 (2025), URL <https://doi.org/10.1038/s41467-025-56759-0>.
- [34] S. Lemieux, S. A. Jalil, D. N. Purschke, N. Boroumand, T. J. Hammond, D. M. Villeneuve, A. Naumov, T. Brabec, and G. Vampa, *Nature Photonics* **19**, 767 (2024), URL <https://doi.org/10.1038/s41566-025-01673-6>.
- [35] D. Theidel, V. Cotte, P. Heinzel, H. Griguer, M. Weis, R. Sondenheimer, and H. Merdji, *Phys. Rev. Res.* **7**, 033223 (2025), URL <https://link.aps.org/doi/10.1103/PhysRevRes.7.033223>.
- [36] T. Lamprou et al., *Photonics* **8**, 192 (2021), ISSN 2304-6732.
- [37] L. Cruz-Rodríguez, D. Dey, A. Freibert, and P. Stammer, *Nat. Rev. Phys.* **6**, 691 (2024), URL <https://doi.org/10.1038/s42254-024-00769-2>.
- [38] A. Gombkötő, P. Földi, and S. Varró, *Phys. Rev. A* **104**, 033703 (2021), URL <https://link.aps.org/doi/10.1103/PhysRevA.104.033703>.
- [39] A. Gombkötő, Ph.D. thesis, University of Szeged (2021), URL <https://doktori.bibl.u-szeged.hu/id/eprint/10993/1/main3final.pdf>.
- [40] S. Yi, N. D. Klimkin, G. G. Brown, O. Smirnova, S. Patchkovskii, I. Babushkin, and M. Ivanov, *Phys. Rev. X* **15**, 011023 (2025), URL <https://link.aps.org/doi/10.1103/PhysRevX.15.011023>.
- [41] J. Rivera-Dean et al., *Phys. Rev. B* **109**, 035203 (2024), URL <https://link.aps.org/doi/10.1103/PhysRevB.109.035203>.
- [42] P. Stammer, J. Rivera-Dean, T. Lamprou, E. Pisanty, M. F. Ciappina, P. Tzallas, and M. Lewenstein, *Phys. Rev. Lett.* **128**, 123603 (2022), URL <https://link.aps.org/doi/10.1103/PhysRevLett.128.123603>.
- [43] P. Stammer, *Phys. Rev. A* **106**, L050402 (2022), URL <https://link.aps.org/doi/10.1103/PhysRevA.106.L050402>.
- [44] A. Pizzi, A. Grolach, N. Rivera, A. Nunnenkamp, and

- I. Kaminer, Nat. Phys. **19**, 551 (2023).
- [45] J. Berkheim, E. Bordo, E. Ragonis, L. Merensky, and A. Fleischer, Phys. Rev. Res. **5**, 043138 (2023), URL <https://link.aps.org/doi/10.1103/PhysRevResearch.5.043138>.
- [46] P. Stammer, J. Rivera-Dean, A. S. Maxwell, T. Lamprou, J. Argüello-Luengo, P. Tzallas, M. F. Ciappina, and M. Lewenstein, Phys. Rev. Lett. **132**, 143603 (2024), URL <https://link.aps.org/doi/10.1103/PhysRevLett.132.143603>.
- [47] I. Gonoskov, R. Sondenheimer, C. Hünecke, D. Kartashov, U. Peschel, and S. Gräfe, Phys. Rev. B **109**, 125110 (2024), URL <https://link.aps.org/doi/10.1103/PhysRevB.109.125110>.
- [48] J. Rivera-Dean, Phys. Rev. A **110**, 063704 (2024), URL <https://link.aps.org/doi/10.1103/PhysRevA.110.063704>.
- [49] E. S. Andrianov and O. I. Tolstikhin, Phys. Rev. A **110**, 023115 (2024), URL <https://link.aps.org/doi/10.1103/PhysRevA.110.023115>.
- [50] J. Rivera-Dean, P. Stammer, A. S. Maxwell, T. Lamprou, E. Pisanty, P. Tzallas, M. Lewenstein, and M. F. Ciappina, Phys. Rev. A **109**, 033706 (2024), URL <https://link.aps.org/doi/10.1103/PhysRevA.109.033706>.
- [51] J. Rivera-Dean, H. B. Crispin, P. Stammer, T. Lamprou, E. Pisanty, M. Krüger, P. Tzallas, M. Lewenstein, and M. F. Ciappina, Phys. Rev. A **110**, 063118 (2024), URL <https://link.aps.org/doi/10.1103/PhysRevA.110.063118>.
- [52] A. Gorlach, O. Neufeld, N. Rivera, O. Cohen, and I. Kaminer, Nat. Commun. **11**, 4598 (2020).
- [53] A. Gombkötő, Acta Phys. Pol. A **143**, 347 (2023), URL http://apoll.ifpan.edu.pl/index.php/appa/article/view/143_347.
- [54] C. S. Lange, T. Hansen, and L. B. Madsen, Phys. Rev. A **109**, 033110 (2024), URL <https://link.aps.org/doi/10.1103/PhysRevA.109.033110>.
- [55] S. Wang, S. Yu, X. Lai, and X. Liu, Phys. Rev. Res. **6**, 033010 (2024), URL <https://link.aps.org/doi/10.1103/PhysRevResearch.6.033010>.
- [56] M. Lewenstein, M. Ciappina, E. Pisanty, J. Rivera-Dean, P. Stammer, T. Lamprou, and P. Tzallas, Nat. Phys. **17** (2021).
- [57] J. Rivera-Dean, P. Stammer, E. Pisanty, T. Lamprou, P. Tzallas, M. Lewenstein, and M. Ciappina, J. Comput. Electron. **20**, 1 (2021).
- [58] P. Stammer, T. Fernández Martos, M. Lewenstein, and G. Rajchel-Mieldzio, Quantum Sci. Technol. **9**, 045047 (2024), URL <https://dx.doi.org/10.1088/2058-9565/ad7881>.
- [59] T. Lamprou, J. Rivera-Dean, P. Stammer, M. Lewenstein, and P. Tzallas, Phys. Rev. Lett. **134**, 013601 (2025), URL <https://link.aps.org/doi/10.1103/PhysRevLett.134.013601>.
- [60] J. Rivera-Dean et al., Phys. Rev. A **105**, 033714 (2022), URL <https://link.aps.org/doi/10.1103/PhysRevA.105.033714>.
- [61] E. S. Andrianov and O. I. Tolstikhin, Phys. Rev. A **112**, 013117 (2025), URL <https://link.aps.org/doi/10.1103/3gjp-f7br>.
- [62] J. Argüello-Luengo, J. Rivera-Dean, P. Stammer, A. S. Maxwell, D. M. Weld, M. F. Ciappina, and M. Lewenstein, PRX Quantum **5**, 010328 (2024), URL <https://link.aps.org/doi/10.1103/PRXQuantum.5.010328>.
- [63] I. Gonoskov, C. Hünecke, and S. Gräfe, *Emergence of nonclassical radiation in strongly laser-driven quantum systems* (2025).
- [64] S. de-la Peña, H. Appel, A. Rubio, and O. Neufeld, *Fully quantum theory of strong-field driven tunable entangled multi-photon states in hhg* (2025).
- [65] D. Theidel, M. Nahra, I. Karuseichyk, H. Griguer, M. Weis, and H. Merdji, *Photon anti-bunching and quantum non-gaussianity from high-harmonic generation* (2026).
- [66] A. Gombkötő, A. Czirják, S. Varró, and P. Földi, Phys. Rev. A **94**, 013853 (2016), URL <https://link.aps.org/doi/10.1103/PhysRevA.94.013853>.
- [67] I. Gonoskov, N. Tsatrafyllis, I. Kominis, and P. Tzallas, Sci. Rep. **6**, 32821 (2016).
- [68] N. Tsatrafyllis, I. Kominis, I. Gonoskov, and P. Tzallas, Nat. Commun. **8**, 15170 (2017).
- [69] A. Gombkötő, S. Varró, P. Mati, and P. Földi, Phys. Rev. A **101**, 013418 (2020).
- [70] M. E. Tzur, M. Birk, A. Gorlach, I. Kaminer, M. Krüger, and O. Cohen, Phys. Rev. Res. **6**, 033079 (2024), URL <https://link.aps.org/doi/10.1103/PhysRevResearch.6.033079>.
- [71] A. Gorlach, M. Tzur, M. Birk, M. Krüger, N. Rivera, O. Cohen, and I. Kaminer, Nat. Phys. **19**, 1689 (2023).
- [72] M. Tzur, M. Birk, A. Gorlach, M. Krüger, I. Kaminer, and O. Cohen, Nat. Photonics **17**, 501 (2023).
- [73] P. Stammer, Nat. Phys. **20**, 1040 (2024), URL <https://doi.org/10.1038/s41567-024-02579-w>.
- [74] J. Rivera-Dean, P. Stammer, M. F. Ciappina, and M. Lewenstein, Phys. Rev. Lett. **135**, 013801 (2025), URL <https://link.aps.org/doi/10.1103/4hdl-bdwj>.
- [75] P. Stammer, Phys. Rev. Res. **6**, L032033 (2024), URL <https://link.aps.org/doi/10.1103/PhysRevResearch.6.L032033>.
- [76] R. V. Gothelf, C. S. Lange, and L. B. Madsen, Phys. Rev. A **111**, 063105 (2025), URL <https://link.aps.org/doi/10.1103/PhysRevA.111.063105>.
- [77] S. de-la Peña, O. Neufeld, M. Even Tzur, O. Cohen, H. Appel, and A. Rubio, J. Chem. Theory Comput. **21**, 283 (2025), URL <https://doi.org/10.1021/acs.jctc.4c01206>.
- [78] Y.-B. Wang and X.-B. Bian, Phys. Rev. A **111**, 043111 (2025), URL <https://link.aps.org/doi/10.1103/PhysRevA.111.043111>.
- [79] D. Habibović and D. B. Milošević, Phys. Rev. A **112**, L051103 (2025), URL <https://link.aps.org/doi/10.1103/1fsq-ffsv>.
- [80] P. Stammer, J. Rivera-Dean, M. Ciappina, and M. Lewenstein, *Weak measurement in strong laser field physics* (2025).
- [81] L. Petrovic, P. Stammer, M. Lewenstein, and J. Rivera-Dean, *Generation of circular polarized high-order harmonics from single color quantum light* (2026).
- [82] M. Sennary, J. Rivera-Dean, M. Lewenstein, and M. Hassan, *Ultrafast quantum optics with attosecond control* (2026).
- [83] C. Shao, H. Lu, X. Zhang, C. Yu, T. Tohyama, and R. Lu, Phys. Rev. Lett. **128**, 047401 (2022), URL <https://link.aps.org/doi/10.1103/PhysRevLett.128.047401>.
- [84] C. S. Lange, T. Hansen, and L. B. Madsen, Phys. Rev.

- A **109**, 063103 (2024), URL <https://link.aps.org/doi/10.1103/PhysRevA.109.063103>.
- [85] G. J. Iafrate and V. N. Sokolov, Phys. Rev. A **109**, 012223 (2024), URL <https://link.aps.org/doi/10.1103/PhysRevA.109.012223>.
- [86] Z. Peng, H. Hu, J. Liu, J. Liu, Z. Zhao, and J. Yuan, Phys. Rev. A **108**, 053119 (2023), URL <https://link.aps.org/doi/10.1103/PhysRevA.108.053119>.
- [87] T. Hansen and L. Bojer Madsen, New J. Phys. **26**, 063023 (2024), URL <https://doi.org/10.1088/1367-2630/ad5755>.
- [88] T. Fennel, Nat. Phys. **17**, 1075 (2021).
- [89] P. Tzallas, Nat. Photonics **17**, 463 (2023).
- [90] P. Tzallas, Nat. Phys. **19**, 472 (2023).
- [91] D. Ko and P. Corkum, Nat. Phys. **19**, 1556 (2023).
- [92] M. Ciappina, Nat. Photonics **19**, 666 (2025).
- [93] Biegert, Jens, Europhysics News **55**, 12 (2024), URL <https://doi.org/10.1051/epn/2024105>.
- [94] O. Cohen, *Attosecond path qubits in strong-field physics* (2026).
- [95] R. Raussendorf and H. J. Briegel, Phys. Rev. Lett. **86**, 5188 (2001), URL <https://link.aps.org/doi/10.1103/PhysRevLett.86.5188>.
- [96] D. E. Browne and T. Rudolph, Phys. Rev. Lett. **95**, 010501 (2005), URL <https://link.aps.org/doi/10.1103/PhysRevLett.95.010501>.
- [97] A. Gombkötő, S. Varró, B. G. Puztai, I. Magashegyi, A. Czirják, S. Hack, and P. Földi, Phys. Rev. A **109**, 053717 (2024), URL <https://link.aps.org/doi/10.1103/PhysRevA.109.053717>.
- [98] I. Babushkin, S. Yi, O. Smirnova, and M. Ivanov, in *Conference on Lasers and Electro-Optics Europe & European Quantum Electronics Conference* (2025), p. 1.
- [99] M. S. Bartlett and J. E. Moyal, Math. Proc. Cambridge Philos. Soc. **45**, 545 (1949).
- [100] T. Wasak, P. Szańkowski, P. Ziń, M. Trippenbach, and J. Chwedeńczuk, Phys. Rev. A **90**, 033616 (2014), URL <https://link.aps.org/doi/10.1103/PhysRevA.90.033616>.
- [101] K. V. Kheruntsyan, J.-C. Jaskula, P. Deuar, M. Bonneau, G. B. Partridge, J. Ruaudel, R. Lopes, D. Biron, and C. I. Westbrook, Phys. Rev. Lett. **108**, 260401 (2012), URL <https://link.aps.org/doi/10.1103/PhysRevLett.108.260401>.
- [102] M. Wegener, *Extreme Nonlinear Optics* (Springer Berlin, Heidelberg, 2005).
- [103] J. Wildenauer, J. Appl. Phys. **62**, 41 (1987), ISSN 0021-8979.